Lysine acetylation promotes PALB2 chromatin association to maintain genome stability

Marjorie Fournier[1,*], Jean-Yves Bleuyard[1], Anthony M. Couturier[1], Jessica Ellins[2], Svenja Hester[1,3], Stephen J. Smerdon[4,#], László Tora[5,6,7,8] and Fumiko Esashi[1,*]

[1] Sir William Dunn School of Pathology, University of Oxford, Oxford, OX1 3RE, UK

[2] Department of Biochemistry, University of Oxford, Oxford, OX1 3QU, UK

[3] Advanced Proteomics Facility, University of Oxford, Oxford, OX1 3RE, UK

[4] The Francis Crick Institute, 1 Midland Rd, London, NW1 1AT, UK

[5]Institut de Génétique et de Biologie Moléculaire et Cellulaire, 67404 Illkirch, France

[6]Centre National de la Recherche Scientifique, UMR7104, 67404, Illkirch, France

[7]Institut National de la Santé et de la Recherche Médicale, U1258, 67404, Illkirch, France

[8]Université de Strasbourg, 67404, Illkirch, France

[#] Current address: Institute of Cancer and Genomic Sciences, University of Birmingham, Vincent Drive, Edgbaston, Birmingham, B15 2TT, UK

* Co-correspondence to:

marjorie.fournier@path.ox.ac.uk and fumiko.esashi@path.ox.ac.uk

Keywords: PALB2, acetylation, chromatin, DNA damage response, genome stability

Abstract

The tumour suppressor PALB2 stimulates error-free DNA repair by homologous recombination (HR). It also associates with actively transcribed chromatin and protects these regions from DNA damage. However, the mechanism by which PALB2 switches between these functions remains enigmatic. Here, we show that the PALB2 chromatin association motif (ChAM), which directly binds to nucleosomes, is targeted by acetylation at a cluster of seven lysine residues (the '7K-patch'). ChAM acetylation within the 7K-patch enhances its nucleosome binding, while limiting its non-specific DNA binding. Importantly, ChAM acetylation is rapidly removed upon DNA damage, resulting in reduced PALB2 chromatin association and increased mobility within the nucleus. The 7K-null mutation confers HR deficiency, including increased sensitivity to the anti-cancer drug Olaparib. Thus, our findings reveal a unique mechanism mediated by acetylation of non-histone protein, which regulates the chromatin interaction of PALB2 to orchestrate efficient DNA repair in human cells and hence promotes genome stability.

Introduction

PALB2, the partner and localizer of the breast cancer susceptibility 2 protein (BRCA2)[1], plays essential roles in the maintenance of cellular homeostasis and disease prevention in humans. Biallelic mutations in *PALB2* are known to cause Fanconi anaemia (FA), a rare genetic disorder characterized by bone marrow failure, developmental abnormalities, and increased incidence of childhood cancers[2,3]. Hereditary monoallelic *PALB2* mutations are also associated with predisposition to breast and pancreatic cancer[4,5], similarly to inherited *BRCA1* and *BRCA2* mutations[6]. At the molecular level, PALB2, BRCA1, and BRCA2 function together to promote the repair of highly genotoxic double-strand DNA breaks (DSBs) by homologous recombination (HR). HR is an error-free repair mechanism that uses the replicated sister chromatid as a repair template and is primarily catalyzed by the RAD51 recombinase. Current models propose that PALB2 is recruited to sites of DNA damage in a manner dependent on BRCA1[7]. Subsequently, a fraction of BRCA2 in complex with RAD51 is mobilized and, in this way, promotes homology search on the sister chromatid, strand invasion, and DNA repair synthesis[1,7]. Importantly, we have previously found that PALB2 functions beyond DSB repair. In undamaged cells, PALB2 constitutively associates with actively transcribed genes and protects these regions from DNA damage arising from replication stress, such as collisions between the transcription and replication machineries[8]. However, while the role of PALB2 in genome stability control is well established, the regulatory mechanisms by which PALB2 promotes HR repair remain elusive.

The ability of PALB2 to associate with chromatin is central to its function. PALB2 associates with active genes through its interaction with MORF-related gene on chromosome 15 (MRG15), a chromodomain-containing protein and reader of histone H3

trimethylated at lysine 36 (H3K36me3) that marks active transcription[8-10]. Additionally, the chromatin-association motif (ChAM), an evolutionarily highly conserved domain uniquely found in PALB2 orthologues, mediates direct interaction with nucleosomes[11]. ChAM is required for the efficient repair of DNA damage induced by the DNA crosslinking agent mitomycin C (MMC)[8,11] or the topoisomerase inhibitor camptothecin (CPT)[8], as well as for optimal DNA stress signaling[12]. Intriguingly, previous observations suggest that PALB2 chromatin association changes dynamically upon DNA damage. Indeed, chromatin immunoprecipitation coupled with quantitative real-time PCR (ChIP-qPCR) revealed that CPT treatment reduced PALB2 association with genic regions, which was concurrent with decreased PALB2-MRG15 interaction and increased PALB2-RAD51 binding[8]. Nonetheless, the molecular mechanisms governing such a dynamic chromatin association remain unknown.

The DNA damage response (DDR) is orchestrated by numerous reversible post-translational modifications (PTMs), including phosphorylation, ubiquitylation, SUMOylation, poly(ADP-ribosyl)ation, methylation, and acetylation (reviewed in[13]). For example, damage-induced PALB2 phosphorylation at residues S59, S177, and S376, mediated by the DNA damage signalling kinases ATM and ATR, facilitates PALB2-BRCA1 interaction and RAD51 foci formation in the DDR[14-16]. Conversely, G1-specific PALB2 ubiquitylation by the E3 ligase KEAP1-CUL3-RBX1 at residue K25 suppresses its interaction with BRCA1, and hence restricts HR[17]. We recently identified PALB2 as a substrate of the lysine acetyltransferases (KATs) GCN5/KAT2A and PCAF/KAT2B[18], two well-known transcriptional regulators that also function in DNA replication and DNA repair (reviewed in[19]). However, it is currently unknown whether lysine acetylation plays a role in regulating PALB2 functions.

The function of KAT2 is closely linked to metabolic signalling since their enzymatic activity requires the metabolite acetyl coenzyme A (acetyl-CoA) as a cofactor[20], suggesting that they may fine-tune cellular processes through target acetylation in accordance with the metabolic status of the cell[21]. Importantly, cancer cells are characterised by both reprogrammed metabolism and elevated genome instability. Nutrient limitations in the tumour microenvironment can increase genome instability[22], which is associated with malignant transformation and resistance to cancer therapy. It is therefore conceivable that cancer cell metabolism alters the landscape of post-translational modification of proteins involved in genome stability maintenance, thus exacerbating genome instability. Based on this premise, the study of KAT-mediated lysine acetylation in genome stability maintenance could reveal molecular mechanisms by which reprogrammed metabolism enhances genome instability in cancer cells and contributes to malignant transformation.

In this study, we investigated the role of KAT2A/B-mediated lysine acetylation in the regulation of PALB2 chromatin association. We showed that KAT2A/B could acetylate a cluster of seven lysine residues (the 7K-patch) within PALB2 ChAM, which enhanced its association with chromatin. Furthermore, DNA damage-induced deacetylation led to chromatin dissociation and increased PALB2 mobility. At the cellular level, lysine to glutamine (Q) substitutions in the 7K-patch resulted in the inability of PALB2 to associate with either nucleosomes or DNA, and severely compromised its function in the DDR. Our findings highlight the importance of acetylation-regulated PALB2 chromatin association in genome stability maintenance.

Materials and Methods

Cell culture and cell lines

All cells were grown at 37°C in an incubator with a humidified atmosphere with 5% CO_2. HEK293T cells were grown in Dulbecco's Modified Eagle's Medium (DMEM, Sigma) supplemented with 10% fetal bovine serum (FBS), 100 U/mL penicillin, and 0.1 mg/mL streptomycin. U2OS Flp-In T-REx P2shRNA cells[8], carrying a doxycycline-inducible shRNA targeting the endogenous *PALB2* 3' UTR, were used to generate stable isogenic cell lines with constitutive expression of N3xFLAG-PALB2 variants. U2OS Flp-In T-REx P2shRNA cells were co-transfected with pOG44 and pcDNA5/FRT GW/N3×FLAG-PALB2 (7Q or 7R), and recombinant stable cell lines were selected in DMEM supplemented with 10% FBS, 100 U/mL penicillin, 0.1 mg/mL streptomycin, 10 μg/mL blasticidin, 200 μg/mL hygromycin B (100 μg/mL to maintain the cell lines), and 1 μg/mL puromycin. Stable U2OS Flp-In T-REx P2shRNA cells lines carrying the empty pcDNA5/FRT GW/N3×FLAG vector or the pcDNA5/FRT GW/N3×FLAG-PALB2 WT vector have been previously described[8]. EUFA1341 cells were transfected with pCEP4-FLAG PALB2 WT or 7R, and stable cell lines expressing FLAG-PALB2 constructs were isolated following hygromycin selection (300 μg/mL) and later maintained using 150 μg/mL hygromycin.

Antibodies

The primary antibodies used (with their respective working dilutions) were against: FLAG (Sigma F1804, mouse, WB: 1/1000), pan-acetyl lysine (AcK) (Cell Signaling Technology (CST) 9441S, rabbit, WB: 1/1000), PALB2 (Bethyl A301-246A, rabbit, WB: 1/500), BRCA2 (Millipore OP95, mouse, WB: 1/1000), RAD51 (Yata *et al.*[23], rabbit, 7946 IF: 1/1000), Lamin A (Sigma L1293, rabbit, WB: 1/2000), γ-H2AX (Millipore 05-636, mouse, WB: 1/1000), GFP (Sigma G1544, mouse, WB: 1/1000), H3 (Bethyl A300-823A, rabbit, WB: 1/1000), GST (Santa Cruz Biotechnology sc-138, mouse, WB:1/1000), Biotin-

HRP conjugated (Sigma A0185, mouse, WB:1/1000), KAT2A/GCN5 (CST 3305, rabbit, WB:1/1000), α-Tubulin (CST 3873, mouse, WB: 1/2000). Secondary antibodies coupled with horseradish peroxidase (HRP): goat anti-mouse (Dako P0447, WB:1/1000), goat anti-rabbit (Dako P0448, WB:1/1000).

DNA damage and cell treatment

For ionising radiation-induced DNA damage, cells were exposed to a 4 Gy dose of γ-rays using a ^{137}Cs source, delivering a dose rate of 1.68 Gy/min (Gravatom). For treatment with either MMC (Sigma M0503) or Olaparib (Enzo Life Sciences LKT-O4402), cells were incubated for 2 h at 37°C with either 1 mM MMC or 2.5 μM Olaparib. DMSO was used as negative vehicle control for Olaparib treatment. KDAC inhibition was performed by treating cells with 5 mM sodium butyrate (NaB, Sigma 303410), 5 μM trichostatin (TSA, Sigma T8552) and 0.5 mM nicotinamide (NaM) for 2 h at 37°C.

siRNA treatment

For KAT2A/GCN5 and KAT2B/PCAF knockdowns, U2OS cells at 30% confluence were transfected using DharmaFECT (Dharmacon) according to the manufacturer's instructions, with 50 pmol each of ON-Targetplus SMARTpools siRNAs targeting KAT2A (Dharmacon L-009722-02-0005) and KAT2B (Dharmacon L-005055-00-0005) in serum-free DMEM. As a negative control, 100 pmol of ON-TARGETplus non-targeting pool siRNAs (Dharmacon D001810-10-05) were used. The serum-free medium was replaced with DMEM supplemented with 10% FBS 24 h after transfection, and the cells were collected by trypsinisation, 72 h after transfection.

Fluorescence recovery after photobleaching (FRAP)

For FRAP experiments, cells were plated into CELLview cell culture dishes (Greiner Bio-One) and analysed in phenol red-free Leibovitz's L15 medium (Gibco). FRAP experiments were performed on a spinning-disk confocal microscope (Ultra-View Vox, Perkin Elmer)

mounted on an IX81 Olympus microscope with an Olympus 60x 1.4 oil PlanApo objective, in a controlled chamber at 37°C and 5% CO_2 (TOKAI HIT stage top incubator). The fluorescence signal was detected using an EMCCD camera (ImagEM, Hamamatsu C9100-13). Cells were bleached in the GFP channel at maximum laser power with a single pulse for 20 ms, within a square region of interest of 5 μm^2. After bleaching, GFP fluorescence recovery was monitored within the bleached area every second for 40 s. FRAP parameters were controlled using Volocity software 6.0 (QuorumTechnologies). FRAP data were fitted and normalised using the FRAP plugins in Image J/Fiji[24]. From the FRAP curve fitting, half-time recovery time values after photobleaching ($t_{1/2}$) were extracted and plotted in Prism 7.02 in which statistical analyses were performed. Normalised fluorescence intensity after photobleaching was calculated by dividing the fluorescence intensity at the bleached area by the whole cellular fluorescence intensity.

Protein purification

Flag-KAT2A, Flag-KAT2A catalytic mutant, and Flag-KAT2B proteins were purified as described in Fournier *et al.*[18]. GST-PALB2 full-length and fragments were purified from 1 L of ArcticExpress cells (Agilent Technologies), grown at 37°C in LB broth medium containing 50 µg/mL ampicillin and 25 µg/mL gentamycin. Protein expression was induced in the presence of 0.1 mM IPTG for 24 h at 13°C. Cells we collected by centrifugation for 15 min at 1,400 × *g* at 4°C and washed with ice-cold phosphate-buffered saline (PBS). Cells lysis was performed by 30 min incubation on ice in 15 mL of ice-cold extraction buffer (50 mM Tris-HCl pH 8.0, 150 mM KCl, 1 mM EDTA, 2 mM DTT, 10% glycerol, and protease inhibitor cocktail (PIC, Sigma P2714) supplemented with 2 mg/mL Lysozyme (Sigma) and 0.2% Triton X-100, followed by sonication. Cell lysates were collected after 45 min centrifugation at 35,000 × *g*, 4°C. GST-fusion proteins were pulled-down with glutathione Sepharose 4B beads (GE Healthcare), pre-washed with ice-cold

PBS. After overnight incubation at 4°C on a rotating wheel, beads were washed three times with ice-cold extraction buffer, three times with 5 mL of ice-cold ATP-Mg buffer (50 mM Tris-HCl pH 7.5, 500 mM KCl, 2 mM DTT, 20 mM $MgCl_2$, 5 mM ATP, and 10% glycerol) and three times with ice-cold equilibration buffer (50 mM Tris-HCl pH 8.8, 150 mM KCl, 2 mM DTT, and 10% glycerol). Proteins were eluted from beads in ice-cold elution buffer (50 mM Tris-HCl pH 8.8, 150 mM KCl, 2 mM DTT, 0.1% Triton X-100, 25 mM L-glutathione, and 10% glycerol).

For GFP-ChAM purification for mass spectrometry analysis, HEK293T cells (3×10^7 cells) transiently expressing GFP-ChAM were collected by centrifugation for 5 min at 500 × *g*, 4°C and washed into ice-cold PBS. Cells were further resuspended in 5 mL ice-cold sucrose buffer (10 mM Tris-HCl pH 8.0, 20 mM KCl, 250 mM sucrose, 2.5 mM $MgCl_2$, 10 mM Benz-HCl and PIC). After addition of 10% Triton X-100 (Sigma) to a final concentration of 0.3%, the cell suspension was vortexed four times for 10 s with 1 min intervals. The intact nuclei were collected by centrifugation for 5 min at 500 × *g*, 4°C, and the supernatant was discarded. The nuclear pellet was washed once with ice-cold sucrose buffer and resuspended in ice-cold NETN250 buffer (50 mM Tris-HCl pH 8.0, 250 mM NaCl, 2 mM EDTA, 0.5% NP-40, 10 mM Benz-HCl and PIC). After 30 min incubation on ice, the chromatin fraction was collected by centrifugation for 5 min at 500 × *g*, 4°C, washed once with 5 mL ice-cold NETN250 buffer and lysed for 15 min at room temperature (RT) in ice-cold NETN250 buffer supplemented 5 mM $MgCl_2$ and 125 U/mL Benzonase. After addition of EDTA and EGTA to respective final concentrations of 5 mM and 2 mM to inactivate the Benzonase, the solubilised chromatin was centrifuged for 30 min at 16,100 × *g*, 4°C and the supernatant was collected as the chromatin-enriched fraction. GFP-ChAM were pull-down using 15 µL GFP-Trap Agarose, pre-washed three times with ice-cold NETN250 buffer and blocked for 3 h at 4°C on a rotating wheel with 500 µL ice-

cold NETN250 buffer supplemented with 2 mg/mL bovine serum albumin (BSA, Sigma). After 3 h protein binding at 4 °C on a rotating wheel, the GFP-Trap beads were collected by centrifugation for 5 min at 1,000 × *g*, 4°C and washed four times with ice-cold NETN250 buffer.

For the analysis of ChAM acetylation upon DNA damage, a GFP-ChAM fusion was transiently expressed from the pDEST53-GFP-ChAM vector for 24 h in HEK293T cells. Whole-cell extracts (WCE) were prepared from ~1.5 × 10^7 cells resuspended in NETN150 buffer (50 mM Tris-HCl pH 8.0, 150 mM NaCl, 2 mM EDTA and 0.5% NP-40 alternative (NP-40 hereafter) (Millipore 492018)) supplemented with 1 mM DTT, PIC, lysine deacetylase inhibitor (5 mM NaB), 1 mM $MgCl_2$ and 125 U/mL benzonase (Novagen 71206-3). After 30 min of incubation on ice, cell debris was removed by 30 min centrifugation at 4°C, and the supernatant was collected as WCE. WCE was then incubated with 15 µl of GFP-Trap Agarose (Chromotek) for GFP-pull down. After 1 h protein binding at 4°C on a rotating wheel, GFP-Trap beads were collected by 5 min centrifugation at 500 × *g* at 4°C and washed three times with NET150 buffer (50 mM Tris-HCl pH 8.0, 150 mM NaCl and 2 mM EDTA) supplemented with 0.1% NP-40, 1 mM DTT, 1X protease inhibitor cocktail, 5 mM NaB and 1 mM $MgCl_2$. Proteins were eluted off beads after boiling them for 10 min at 85°C in Laemmli buffer supplemented with 10 mM DTT. The proteins were separated by SDS-PAGE and analysed by western blot.

For the nucleosome pull-down assays, GFP-ChAM variants were affinity-purified from HEK293T cells (3 × 10^7 cells) following transient expression. After collecting cells by centrifugation for 5 min at 500 × *g*, 4°C, the cell pellet was washed twice with ice-cold PBS and resuspended in ice-cold NETN150 buffer supplemented with 10 mM benzamidine hydrochloride (Benz-HCl) and PIC. After 30 min incubation on ice, the chromatin was pelleted by centrifugation for 5 min at 500 × *g*, 4°C, and the supernatant was collected as

NETN150 soluble fraction and centrifuged for 30 min at 16,100 × *g*, 4°C to remove cell debris and insoluble material. For each sample, 10 µL of GFP-Trap Agarose were washed three times with 500 µL ice-cold NETN150 buffer. NETN150 soluble proteins (2.5 mg) in a total volume of 1 mL ice-cold NETN150 buffer were incubated with the GFP-Trap beads to perform a GFP pull-down. After 2 h protein binding at 4°C on a rotating wheel, the GFP-Trap beads were collected by centrifugation for 5 min at 500 × *g*, 4°C and washed four times with ice-cold NETN150 buffer. Human nucleosomes were partially purified from HEK293T cells (4×10^7 cells), collected by centrifugation for 5 min at 500 × *g*, 4°C, washed twice with ice-cold PBS and lysed in ice-cold NETN150 buffer supplemented with 10 mM Benz-HCl and PIC). After 30 min of incubation on ice, the chromatin was pelleted by centrifugation for 5 min at 500 × *g*, 4°C, washed once with ice-cold NETN150 buffer and digested for 12 min at 37 °C with 50 gel units of micrococcal nuclease (NEB) per milligram of DNA in NETN150 buffer containing 5 mM $CaCl_2$, using 200 µL buffer per mg of DNA. The reaction was stopped with 5 mM EGTA and the nucleosomes suspension cleared by centrifugation for 30 min at 16,100 × *g*, 4°C.

Acetyltransferase assays

Radioactive ^{14}C-acetyltransferase assays on recombinant proteins were performed by incubating purified GST-PALB2 (full length and fragments) or purified RAD51 with purified FLAG-KAT2B in the presence of ^{14}C-labeled acetyl-CoA. The reaction buffer contained 50 mM Tris-HCl pH 8.0, 10% glycerol, 100 mM EDTA, 50 mM KCl, 0.1 M sodium butyrate, protease inhibitor cocktail, and 5 mM DTT. Reactions were incubated for 1 h at 30°C, stopped by addition of Laemmli buffer containing 10%-mercaptoethanol, boiled for 5 min, resolved by SDS-PAGE, and stained using Coomassie blue to reveal overall protein distribution. The acrylamide gel containing proteins was then dried and exposed to phosphorimager to reveal ^{14}C-labeled proteins. Non-radioactive acetyltransferase assays

were performed as described above using cold acetyl-CoA instead. After 1 h incubation at 30°C, the reactions were stopped by addition of Laemmli buffer containing 10 mM DTT, boiled for 5 min, resolved by SDS-PAGE, and analysed by western blot using anti-acetyl lysine antibodies, after Ponceau S staining of the membrane to reveal overall protein distribution. Acetyltransferase assays performed for mass spectrometry analyses were performed as described in Fournier *et al.*[18].

Nucleosome pull-down assay

Nucleosome pull-down assays were performed by mixing in NETN150 buffer supplemented with 2 mg/mL BSA, 250 µg of partially purified nucleosomes and GFP-ChAM variants immobilised on GFP Trap beads, followed by 30 min incubation at RT, then 1.5 h incubation at 4 °C, on a rotating wheel. GFP-Trap beads were further washed four times with NETN150 buffer, and samples were analysed by SDS-PAGE and western blot.

DNA binding assays

For ChAM peptides binding to DNA, proteins or peptides were incubated in NDTN150 buffer (50 mM Tris HCl pH 7.5, 150 mM NaCl, 0.5% NP-40 and 2 mM DTT) in the presence of 300 ng pBluescript plasmid DNA for 1 h at RT. Reactions were loaded onto a 1% agarose Tris-Acetate-EDTA (TAE) gel and run at 100 V for 60 min. The gel was stained for 1 h at RT using 0.5 µg/mL ethidium bromide in Tris-Borate-EDTA (TBE) buffer. Binding of ChAM peptide to histone H3 was performed by incubating for 1 h at 4°C biotinylated ChAM peptides and histone H3 protein in NDTN250 buffer (50 mM Tris HCl pH 7.5, 250 mM NaCl, 0.5% NP-40, and 2 mM DTT) supplemented with 5 mg/mL BSA. Dynabeads MyOne T1 blocked with BSA in NDTN250 buffer were added to the peptide-Histone H3 mixture and incubated for 1 h at 4°C. Immobilised complexes were washed three times with NDTN250 buffer and proteins were visualised by western blotting using the indicated antibodies.

Immunofluorescence microscopy

For γ-H2AX foci analysis, cells were grown on coverslips and washed with PBS before pre-extraction with 0.1% Triton in PBS for 30 s at RT. Cells were then fixed twice with 4% PFA in PBS, first for 10 min on ice and then for 10 min at RT. After permeabilisation in 0.5% Triton X-100 in PBS for 10 min at RT, cells were blocked with 5% BSA in PBS-0.1% Tween 20 solution and incubated with anti-γ-H2AX primary antibodies (see antibodies section) for 3 h at RT. After washing with PBS-0.1% Tween 20 for 5 min at RT, cells were incubated with secondary antibodies coupled with a fluorophore, washed with PBS-0.1% Tween 20 for 5 min at RT, and mounted on slides using a DAPI-containing solution. For RAD51 foci analysis, cells were grown on coverslips and washed twice with PBS before fixation with 4% PFA in PBS for 15 min at RT. After washing twice with PBS, cells were permeabilised with PBS-0.5% Triton X-100 for 5 min at RT and blocked with 3% BSA in PBS-0.1% Triton X-100 before incubation with anti-RAD51 primary antibodies (see antibodies section) for 2 h at RT. After washing three times with PBS-0.5% Tween 20, cells were incubated with secondary antibodies coupled with a fluorophore, washed three times with PBS-0.5% Tween 20 and mounted on slides using a DAPI-containing solution. Cells were analysed on a spinning-disk confocal microscope (Ultra-View Vox, Perkin Elmer) mounted on an IX81 Olympus microscope, with a 40x 1.3 oil UPlan FL objective. The fluorescence signal was detected using an EMCCD camera (ImagEM, Hamamatsu C9100-13). Images were processed in Image J (https://imagej.nih.gov/ij/)[25] .

Sequence alignment analysis

Sequences of PALB2 orthologues from 12 species were retrieved from the Ensembl (http://www.ensembl.org) and NCBI (https://www.ncbi.nlm.nih.gov) resources and aligned using MUSCLE (http://www.ebi.ac.uk/Tools/msa/muscle/). Hs (Homo sapiens, human), Pt (Pan troglodytes, Chimpanzee), Pp (Pan paniscus, Bonobo), Bt (Bos taurus,

Cow), Ml (Myotis lucifugus, Little brown bat), Ss (Sus scrofa, Wild boar), Ec (Equus caballus, domesticated horse), Clf (Canis lupus familiaris, Dog), Am (Ailuropoda melanoleuca, Giant panda), Oa (Ornithorhynchus anatinus, Platypus) Gg (Gallus gallus, Chicken), and Tg (Taeniopygia guttata, Zebra finch).

Results

PALB2 diffusion rate increases upon DNA damage and protein deacetylation

To investigate the spatio-temporal dynamics of PALB2 in the DDR, we used fluorescence recovery after photobleaching (FRAP) in cells stably expressing a PALB2 fusion with FLAG and EGFP (FE-PALB2). We first assessed the diffusion kinetics of FE-PALB2 in cells treated with ionising radiation (IR), MMC, or the PARP inhibitor Olaparib. The induction of DNA damage was monitored using serine 139 phosphorylated histone variant H2AX (γ-H2AX) foci formation, a marker for DNA damage signalling (Fig. S1A). Remarkably, FE-PALB2 diffusion rate, as defined by the half-recovery time ($t_{1/2}$) after photobleaching, was significantly increased in all tested DNA damaging conditions. Compared to untreated control conditions, IR, MMC, and Olaparib treatment decreased FRAP $t_{1/2}$ by 22%, 36%, and 18%, respectively (Fig. 1A-D and Supplementary Fig. 1A-C).

We reasoned that damage-induced changes in FE-PALB2 dynamics could be mediated by reversible PTMs. Importantly, our previous lysine acetylome study highlighted PALB2 as a protein which was acetylated in HeLa cells, but not upon depletion of KAT2A and KAT2B[18] (hereafter KAT2A/B). Motivated by this observation, we examined whether KAT2A/B were involved in the regulation of PALB2 dynamics. Strikingly, KAT2A/B down-regulation led to an increase in FE-PALB2 diffusion (i.e., reduced FRAP $t_{1/2}$) (Fig. 1E, F and Supplementary Fig. 1D, E), concomitant with reduced

levels of global acetylation[18]. Conversely, the diffusion rate of FE-PALB2 was significantly decreased (i.e., increased FRAP $t_{1/2}$) upon lysine deacetylase (KDAC) inhibition, which increased the global level of lysine acetylation (Fig. 1G, H and Supplementary Fig. 1F, G). Together, these results suggested that PALB2 dynamics was increased upon DNA damage and by suppressing lysine acetylation events.

KAT2A/B acetylates PALB2 within its ChAM, which is deacetylated upon DNA damage

To address the molecular mechanism by which lysine acetylation regulates the dynamics of PALB2, we next mapped the residues modified by KAT2A/B. Our previous shotgun mass spectrometry (MS) analysis of the endogenous acetylome revealed that lysine residues within the central region of PALB2 were frequently acetylated in a KAT2A/B-dependent manner (Fig. 2A). To verify that KAT2A/B could directly acetylate PALB2, we performed *in vitro* acetylation assays using either recombinant full-length PALB2 or a series of PALB2 fragments (Fig. 2A) with purified KAT2A or KAT2B, and detected acetylation by ^{14}C-autoradiography (Fig. 2B) or western blot (WB) against acetylated lysine (pan-AcK) (Supplementary Fig. 2). Lysine acetylation of full-length PALB2 and fragment 2, which encompasses the central region of PALB2 (residues 295-610), was clearly visible following *in vitro* acetylation with KAT2A (Supplementary Fig. 2B) or KAT2B (Fig. 2B and Supplementary Fig. 2A), but not with a catalytically inactive mutant of KAT2A (Supplementary Fig. 2B).

Our tandem MS analysis of *in vitro* acetylated PALB2 identified acetylation events enriched at lysine residues within PALB2 ChAM (Fig. 2A, C). A similar acetylation pattern was detectable in an extended ChAM fragment (PALB2 residues 353-499, corresponding to fragment #5 in Fig. 3A), which was expressed in HEK293T cells and purified from

chromatin-enriched fraction (Fig. 2D). Acetylated residues within ChAM were mapped to a cluster of seven lysine residues (denominated the 7K-patch), composed of K436, K437, K438, K441, K443, K445, and K449. All MS/MS spectra for acetylated PALB2 peptides are provided in the supplementary material. Importantly, ChAM was rapidly deacetylated upon IR treatment (within 15 min) and remained deacetylated for at least 2 h (Fig. 2E). Collectively, our results reveal a changing pattern of PALB2 acetylation in human cells whereby the ChAM is highly acetylated in normally growing cells but rapidly deacetylated upon DNA damage.

ChAM acetylation regulates PALB2 chromatin association

The identification of lysine acetylation within ChAM was particularly interesting since acetylation-mediated regulation of ChAM function could explain the changes in PALB2 diffusion rate detectable by FRAP (Fig. 1), as well as the damage-induced PALB2 release from actively transcribed genes shown previously using ChIP-qPCR[8]. Encouraged by these observations, we next examined the impact of the 7K-patch on ChAM chromatin association. Analysis of the chromatin fraction of HEK293T cells expressing GFP fusions of various ChAM truncations revealed that the region containing the 7K-patch was essential for its chromatin enrichment (Fig. 3A, B). To eliminate the possibility that reduced chromatin enrichment resulted from mislocalisation of the 7K-patch-deleted variants to the cytoplasm, we assessed *in vitro* the direct interaction between the same fragments purified from the soluble fraction of HEK293T cells and separately prepared human nucleosomes. The pull-down assay showed that, indeed, deletion of the 7K-patch led to impaired ChAM interaction with nucleosomes (Fig. 3C).

To assess the role of acetylation within the 7K-patch in ChAM nucleosome binding, we next used synthetic ChAM peptides (PALB2 residues 395-450) acetylated at

evolutionarily conserved lysine residues within the 7K-patch, K436, K437, and K438 (Fig. 2A, D). Our *in vitro* nucleosome binding assays revealed that ChAM binding to nucleosomes was modestly enhanced by acetylation at K436, K437, or K438 compared to the non-acetylated ChAM peptide (Fig. 3D). Remarkably, we found that, in the presence of excess salmon sperm DNA, non-acetylated ChAM lost its ability to bind nucleosomes, while acetylated ChAM maintained its association. The effect was most prominent with K438 acetylation, which was detected in our previous MS study of the endogenous HeLa KAT2A/B-acetylome. We surmise that non-specific electrostatic interactions between DNA and the non-acetylated lysine residues (K441, K443, K445, and K449) in the vicinity of the acetylated residues contributes to overall binding but is titrated out in the presence of excess salmon sperm DNA. These observations suggest that acetylated ChAM residues mediate specific interaction with the histone core.

Considering the likely interaction between the positively charged 7K-patch and negatively charged DNA, we next assessed the impact of acetylation at K436, K437, and K438 on ChAM binding to DNA. As anticipated, lysine acetylation, which neutralises the positive charge on the lysine side chain, abolished ChAM interaction with DNA (Fig. 3E, F). These results suggested that the 7K-patch plays an important role in regulating the mode of ChAM chromatin association: acetylation within this region enhanced its unique nucleosome binding properties while reducing its non-specific affinity for DNA. Notably, a PALB2 variant with an internal deletion of the ChAM domain, which abolishes PALB2 chromatin association[11], showed a significant increase in PALB2 diffusion rate, as defined by reduced FRAP $t_{1/2}$ (Supplementary Fig. 3). This observation suggested that increased PALB2 mobility reflected the chromatin-free fraction of PALB2. Altogether, these observations support the notion that ChAM acetylation facilitates PALB2 chromatin association and restricts its mobility.

The ChAM 7K-patch regulates PALB2 chromatin association

We next aimed to assess the physiological impact of 7K-patch acetylation *in vivo*. With this in mind, we first examined the biochemical properties of ChAM variants in which lysine residues within the 7K-patch were substituted to glutamine. K to Q substitutions neutralise the charge and are hence widely used to mimic lysine acetylation (Supplementary Fig. 4A). We generated recombinant GST-fusions of ChAM WT and mutants harboring Q substitutions at all seven lysine residues (7Q), three conserved lysine residues, K436, K437, and K438 (3Q4K), or the four remaining lysine residues, K441, K443, K445, and K449 (3K4Q) within the 7K-patch (Fig. 4A, B). Unexpectedly, *in vitro* nucleosome binding assays showed that all variants with Q substitutions abolished ChAM interaction with nucleosomes (Fig. 4C). This observation appeared to be at odds with our findings that ChAM acetylation enhanced nucleosome binding (Fig. 3D) and that PALB2 mobility increased upon KAT2A/B inhibition or induction of DNA damage, which coincided with reduced ChAM acetylation (Fig. 1D-H and Fig. 2E). Glutamine has a shorter side chain than a *bona fide* acetylated lysine (Supplementary Fig. 4A); hence, we reasoned that, while mimicking the charge neutralisation of lysine acetylation, it may hinder nucleosome binding. These observations, therefore, suggest that the interpretation of data resulting from K to Q substitutions as acetyl-mimetic may be misleading in certain contexts. As anticipated from the change in electrostatic charge, all ChAM variants with K/Q substitutions exhibited an impaired association with DNA (Fig. 4D).

Our biochemical analyses demonstrated that 7Q substitution hindered ChAM ability to associate with both nucleosomes and DNA. Hence, hereafter, we used this variant as a PALB2 ChAM 7K null-mutant and examined how the association of PALB2 with nucleosomes and DNA impacted its dynamics *in vivo*. Along with the 7Q PALB2 variant,

we generated a PALB2 variant in which ChAM 7K residues were substituted to arginine (R). Arginine substitution maintains the overall positive charge but cannot accept acetylation. Cell lines stably expressing GFP-fusions of full-length PALB2 7Q or 7R variants were established, and their dynamics were assessed using FRAP. We found that similarly to PALB2 ChAM deletion mutant (Supplementary Fig. 3), PALB2 7Q mutant exhibited increased diffusion kinetics compared to PALB2 wild-type (WT) and 7R (Fig. 4E, F). In line with this observation, the PALB2 7Q mutant showed significantly reduced enrichment in the chromatin fraction of cells compared to PALB2 WT and 7R (Supplementary Fig. 4B, C). The increased mobility of PALB2 7Q is thus consistent with its impaired chromatin association, potentially reflecting free diffusion in the nucleus. Intriguingly, PALB2 recruitment to DNA damage sites was not hindered by 7Q and 7R mutations, as shown by laser micro-irradiation experiments (Supplementary Fig. 4D, E). Collectively, these observations suggest that lysine residues within the ChAM 7K-patch are essential for regulating PALB2 chromatin association and mobility within cells, but dispensable for promoting its recruitment to sites of DNA damage.

PALB2 ChAM 7K-patch is required to maintain genome stability

To assess the physiological role of the ChAM 7K-patch in the regulation of PALB2 function in the DDR, we established U2OS cell lines in which endogenous *PALB2* can be down-regulated by a doxycycline-inducible short hairpin RNA (U2OS-shPALB2). These include stable lines harbouring an empty vector (EV), as a negative control, or an expression vector for FLAG-tagged full-length PALB2 WT, 7Q or 7R variants. WB analysis confirmed that all cell lines exhibit equivalent levels of FLAG-PALB2 protein expression and efficient depletion of endogenous PALB2 upon doxycycline exposure (Fig. 5A).

The best-characterised function of PALB2 in the DDR is to support RAD51 foci formation and hence facilitate HR repair of DSBs. Endogenous PALB2 depletion in EV cells abolished RAD51 foci formation in both undamaged and DNA damage conditions (Supplementary Fig. 5A). Importantly, damage-induced RAD51 foci formation was efficiently restored in U2OS-shPALB2 cells expressing PALB2 WT or 7R but remained severely impaired in those expressing PALB2 7Q (Fig. 5B, C). Further, U2OS-shPALB2 cells expressing PALB2 7Q exhibited a higher level of sensitivity to Olaparib than their PALB2 WT or 7R expressing counterparts (Fig. 5D). Given that increased sensitivity to PARP inhibition is a hallmark of HR deficiency, this finding suggests that the 7Q substitutions conferred HR defects. Notably, neither PALB2 7R nor 7Q presented defects in their interactions with BRCA2 or RAD51 (Supplementary Fig. 5B). Collectively, these observations support the notion that defective DDR in U2OS-shPALB2 cells expressing PALB2 7Q is caused by its inability to associate with chromatin.

Discussion

In this study, we have demonstrated that reversible PALB2 acetylation controls its mode of chromatin association, which is essential during the DDR: the 7K-patch in the C-terminal part of ChAM was acetylated by KAT2A/B in undamaged cells but deacetylated upon DNA damage. Crucially, ChAM acetylation enhances PALB2 binding to nucleosomes and limits non-specific interactions with DNA. DNA damage, however, triggers PALB2 deacetylation and increases the overall mobility of PALB2. The PALB2 7Q variant, which fails to associate with either nucleosomes or DNA, was markedly unable to support HR, despite its intact interactions with BRCA2 and RAD51 and normal recruitment to sites of DNA damage. Considering all our findings collectively, we propose the model shown in Fig. 6: KAT2A/B-mediated ChAM acetylation, jointly with MRG15, promotes PALB2

enrichment at undamaged transcriptionally active chromatin. DNA damage triggers ChAM deacetylation and a concomitant reduction in PALB2-MRG15 interaction[8], which releases PALB2 from chromatin. In this way, PALB2 may become available to form functional HR complexes with BRCA1, which is otherwise less stably associated with PALB2[8]. Following the recruitment of the entire HR complex to sites of DNA damage, deacetylated ChAM binding to exposed naked DNA may allow appropriate engagement of this complex with damaged DNA, and hence, promote RAD51 loading and HR repair.

The increase in PALB2 dynamics during the DDR shown in this study is reminiscent of previous reports revealing increased RAD51 mobility upon replication stress[26,27]. Yu *et al*. have shown that a fraction of RAD51, which is in complex with BRCA2, is immobile in unchallenged cells, but becomes mobile upon hydroxyurea-induced replicative stress[26]. Notably, their data suggested that such increased RAD51 mobility was unlikely to be a consequence of altered interaction with BRCA2 since no change in RAD51-BRCA2 interaction was detectable upon replicative stress. Similarly, Jeyasekharan *et al*. have reported increased BRCA2 mobility upon IR-induced DNA damage, which was induced in a manner dependent on the DNA damage signalling kinases ATM and ATR and coincided with active HR events[28]. In light of previous observations that BRCA2 and PALB2 form a stable complex (B2P2 complex) together with a fraction of RAD51, and that their interaction is important for HR repair, we propose that the B2P2 complex and associated RAD51 are mobilised together upon genotoxic stress.

The dynamic exchange of HR factors appears to extend beyond damaged chromatin, and our observations raise a fundamental question: what could be the benefit of such a phenomenon in the DDR? One possibility is that the B2P2 complex needs to relocate from undamaged actively transcribed chromatin to sites of DNA damage, a process that likely requires a release of the complex from chromatin[8]. Cells may derive an

advantage by retaining the B2P2 complex readily available and in close proximity to regions highly vulnerable to DNA damage, such that it can be promptly recruited when DNA damage arises, for instance upon replication-transcription collisions. Notably, however, there is an indication that the increase in PALB2 mobility is long-lived; we observed that PALB2 remained less acetylated after DNA damage, and thus in a highly mobile form, for at least two hours after induction of DNA damage. Hence, it is tempting to speculate that increased PALB2 mobility may assist DNA repair over a broader range of time and space. MS-based protein copy number estimates showed that endogenous PALB2 and BRCA2 are stoichiometric, but are significantly less abundant than RAD51[29,30]. It is therefore conceivable that the B2P2 complex acts as a carrier to continually recruit new RAD51 molecules from the free excess pool across the nucleus, following the loading of associated RAD51, throughout the HR process.

The mechanisms that regulate the localisation of HR factors remain incompletely understood but undoubtedly involve PTMs. We propose that variable modes of PTM-mediated chromatin association synergistically govern the recruitment of repair factors to defined regions of chromatin. In unchallenged cells, PALB2 is enriched at actively transcribed chromatin through ChAM acetylation and H3K36me3-mediated MRG15 interaction, while maintaining transient chromatin interaction without stable engagement. This mode of association may allow a severance mechanism, in which PALB2 continuously monitors the presence of DNA damage across these regions. Upon DNA damage, PALB2 may shift to a distinct mode of chromatin association, which allows its recruitment to sites of DNA damage through interaction with BRCA1, fulfilling its function in promoting HR repair. Intriguingly, cells expressing the non-acetylable PALB2 7R variant exhibited no detectable HR defects. While this observation is compatible with our finding that ChAM is deacetylated upon DNA damage, our preliminary results also suggest

that this variant may have limited capacity in the surveillance mechanism in undamaged cells. Indeed, cells expressing PALB2 7R exhibited an increase in the basal level of γ–H2AX compared to those expressing PALB2 WT (data not shown), highlighting the importance of PALB2 acetylation in unperturbed cells. Our work also suggests that caution should be exercised in the use of K to Q substitutions for functional studies of lysine acetylation. We anticipate that robust *in vivo* assessment of acetylation events may require the development of a chemically modifiable residue, which exhibits improved similarity to acetylated lysine in a reversible manner.

More broadly, lysine acetylation is known to control biological processes (e.g., gene transcription[31]) based on the metabolic status of the cell. Therefore, a better appreciation of the role of lysine acetylation in the DDR could expand the scope of studies aiming to understand how reprogrammed metabolism could increase genome instability in cancer cells[22]. Since PTMs are essential to ensure the maintenance of physiological homeostasis and metabolites are necessary cofactors for the deposition of these PTMs, we envision that reprogrammed metabolism in cancer cells could alter the PTM landscape for proteins involved in the DDR and, hence, contribute to genome instability. In this study, we established that reversible PALB2 acetylation regulates its mobility and function in the DDR. Considering that glucose concentration in the growth medium can influence the level of protein acetylation in cells[31], it will be important to understand whether PALB2 function could be affected by cellular metabolic status. Strikingly, our preliminary results demonstrated that glucose concentration in the growth media does indeed affect PALB2 mobility (data not shown). This observation supports the notion that in tumour cells with reprogrammed metabolism, protein properties (e.g., chromatin association) could be detrimentally altered. Future studies will assess whether aberrant PALB2 lysine acetylation may be detected in cancer tissues and whether this is modulated by KDAC or

bromodomain inhibitors, currently in clinical trials for cancer therapy, or by alteration of glucose metabolic pathways. Furthermore, deciphering the metabolic regulation of the DDR and DNA repair could highlight additional cellular pathways that might be targeted for cancer therapy, possibly in combination with existing therapies that otherwise may give rise to resistance.

Author contributions

M.F. and F.E. conceived the study and designed the experimental strategies; M.F., J-Y.B, A.M.C., J.E., and S.H. performed the experiments; J-Y.B, S.S., and L.T. contributed to reagents and analytical tools; M.F. and J.E. analysed data; M.F., J.Y.B, A.M.C., S.S., and F.E. contributed to text and figures; M.F. and F.E. wrote the manuscript.

Acknowledgements

FE is supported by a Wellcome Trust Senior Research Fellowship in Basic Biomedical Science (101009/Z/13/Z) and is thankful for the support of the Edward P Abraham research fund at the Sir William Dunn School of Pathology, University of Oxford. SJS is supported by the Francis Crick Institute which receives its core funding from Cancer Research UK (FC001156), the UK Medical Research Council (FC001156), and the Wellcome Trust (FC001156). LT receives funding from the European Research Council (ERC) Advanced Grant (ERC-2013-340551, Birtoaction). We are also grateful to Nicola O'Reilly (Francis Crick Institute Peptide Chemistry Technology Platform) for synthesis of ChAM peptides, Andrew Jefferson and Carina Mónico (Micron Oxford Advanced Bioimaging) for assistance with the use of microscope, Christine Ralf (Sir William Dunn School) for technical support in generating constructs, and Chris Norbury (Sir William Dunn School) for critical reading of the manuscript.

Competing interests

The authors declare no financial and non-financial competing interests on this study.

Data availability: The mass spectrometry proteomics data have been deposited to the ProteomeXchange Consortium via the PRIDE[32] partner repository with the dataset identifier PXD014678 and PXD014681.

Figure legends

Figure 1. PALB2 dynamics increases upon DNA damage or deacetylation. The dynamics of FLAG-EGFP (FE)-tagged PALB2 expressed in U2OS Flp-In T-Rex cells was monitored by FRAP. ***A-B.*** Cells were examined under non-treated conditions (NT; blue) or treated with 4 Gy of ionising radiation (IR; green) or 1 mM mitomycin C (MMC; red). ***C-D.*** Cells were treated with the PARP inhibitor Olaparib or DMSO as a control. ***E-F.*** KAT2A and KAT2B were depleted by small interfering RNA treatment (siKAT2A/siKAT2B). Non-treated (NT) and scrambled siRNA (siSCR) treated cells were used as controls. ***G-H***. Lysine deacetylase activity was inhibited (KDACi) using 5 mM sodium butyrate, 5 μM trichostatin A, and 5 mM nicotinamide. DMSO-treated cells were used as control. For each condition, representative images of live cells before bleaching (pre-bleaching) and during a 37.5 s recovery period (post-bleaching) are shown together with half-time recovery plots for at least 20 cells. Dashed circles indicate bleached areas. Statistical analyses were performed using GraphPad Prism 7.02 and *p*-values are for the unpaired Student's *t*-test (** $p < 0.0035$, *** $p < 0.0006$, and **** $p < 0.0001$).

Figure 2. KAT2A/B acetylates PALB2 within its ChAM, which is deacetylated upon DNA damage. ***A.*** KAT2A/B-dependent PALB2 acetylated lysine residues identified by tandem mass spectrometry-based proteomics analyses *in vivo* (blue), *in vitro* (black), or overexpressed ChAM in HEK293T cells (red). Diagram showing GST-tagged full-length PALB2 and fragments purified from *E.coli* and used for *in vitro* acetylation assays. FL: full-length PALB2 (200kDa), 1: PALB2 1-320 (61.2kDa), 2: 295-610 (60.6kDa), 3: 580-900 (61.2 kDa), and 4: 867-1186 (61.1kDa). ***B.*** *In vitro* acetylation of PALB2 FL and fragments 1-4 by FLAG-KAT2B in the presence of ^{14}C-labelled acetyl-CoA. Proteins were separated by SDS-PAGE and visualised by Coomassie Brilliant Blue staining, while acetylated

proteins were detected by ^{14}C-autoradiography. RAD51 is not acetylated by KAT2A/B *in vivo*[18] and was used as a negative control. ***C.*** Acetylated lysine residues identified by tandem-mass spectrometry-based proteomics analysis following *in vitro* acetylation of recombinant PALB2 FL or fragment 2 by FLAG-KAT2B, FLAG-KAT2A, or a catalytically inactive mutant of FLAG-KAT2A. The acetylation level of each residue has been calculated as previously described by Fournier *et al*., 2016[18]. ***D.*** ChAM protein sequences from 12 PALB2 orthologues were aligned using MUSCLE and visualised using ClustalW default colour-coding. Lysine residues acetylated *in vitro* by KAT2A and KAT2B are highlighted with green and red dots, respectively. Lysine residues acetylated *in vivo* following ChAM overexpression are highlighted with blue dots. ChAM C-terminal lysine-rich patch (7K-patch, residues 436-449) is highlighted in red. ***E.*** Cells overexpressing GFP-tagged ChAM were challenged with 4 Gy of IR, and ChAM acetylation status was monitored up to 2 h after irradiation by western blotting. GFP-ChAM and acetylated GFP-ChAM (Ac-GFP-ChAM) were detected using anti-GFP and anti-acetyl lysine antibodies. ϒ-H2AX is shown as a positive control for DNA damaging treatment. The histogram on the bottom shows the relative level of Ac-GFP-ChAM following irradiation. Acetylated and total GFP-ChAM levels were quantified by densitometry analysis, and the acetyl/total GFP-ChAM ratio was normalised to the undamaged condition.

Figure 3. **ChAM acetylation regulates its chromatin association. *A.*** Diagram showing full-length (FL) PALB2 and GFP-ChAM fragments 1 to 5 used in *in vitro* nucleosome binding assays. GFP alone (EV) was used as a negative control. ChAM C-terminal lysine-rich patch (7K-patch, residues 436-449) is highlighted in red. ***B.*** Chromatin association of GFP-ChAM fragments 1 to 5 transiently expressed in HEK293T cells. Empty GFP vector (EV) was used as a negative control. Whole-cell extract was also prepared to compare

GFP-CHAM fragments expression levels. Lamin A and Histone H3 were used as controls for the cellular fractionation. ***C***. *In vitro* nucleosome binding assay for GFP and GFP-ChAM fragments 1 to 5. Partially purified human nucleosomes captured by GFP and GFP-ChAM fragments immobilised on beads were detected by anti-histone H3 western blot and Ponceau S staining. ***D.*** *In vitro* nucleosome binding assays for synthetic Biotin-ChAM peptides non-acetylated or acetylated at single lysine residues 436 (436-ac), 437 (437-ac), and 438 (438-ac), or all three lysine residues (All 3-ac). After incubation in the presence of purified HeLa polynucleosomes, Biotin-ChAM peptides were pulled-down using streptavidin beads (Strep pulldown), and nucleosome binding was assessed by anti-histone H3 western blot. Assays were performed in the absence or presence of 5 µg salmon sperm DNA. ***E.*** Agarose gel mobility shift-assay using 300 ng pBluescript plasmid DNA and increasing amount of non-acetylated (ChAM WT) or tri-acetylated at positions 436/437/438 (ChAM 3ac) synthetic Biotin-ChAM peptides, i.e. 2.97 µM (light gray circle), 5.94 µM (dark gray circle) and 29.7 µM (black circle). Three DNA conformations are indicated: supercoiled (s.c.), linear (l.), and nicked (n.). ***F.*** Agarose gel mobility shift-assay using pBluescript plasmid DNA and non-acetylated (ChAM WT), mono-acetylated at position 436 (436-ac), 437 (437-ac), or 438 (438-ac), or tri-acetylated at positions 436/437/438 (All 3-ac). Three DNA conformations are indicated: supercoiled (s.c.), linear (l.), and nicked (n.).

Figure 4. The ChAM 7K-patch regulates PALB2 chromatin association. ***A.*** Positions of lysine residues within the ChAM 7K-patch, which have been mutated to either arginine (R) or glutamine (Q) for phenotypic analyses. Four constructs have been generated: 7R and 7Q, in which all seven lysine residues of the 7K-patch have been substituted to arginine or glutamine; 3Q4K and 3K4Q, in which the first three and last four lysine

residues of the 7K-patch have been substituted to glutamine, respectively. ***B.*** GST, GST-ChAM WT, 3Q4K, 3K4Q, and 7Q proteins purified from *E.coli* and analysed by SDS-PAGE and Coomassie blue staining. ***C.*** *In vitro* binding assays using immobilised GST-ChAM WT, 3Q4K, 3K4Q, and 7Q and purified HeLa mononucleosomes. GST was used as a negative control. The nucleosome binding efficiency was assessed by anti-histone H3 western blotting. ***D.*** Agarose gel mobility shift-assay using pBluescript plasmid DNA (pBS) and purified GST-ChAM WT, 3Q4K, 3K4Q, and 7Q. Three DNA conformations are indicated: supercoiled (s.c.), linear (l.), and nicked (n.). ***E-F.*** FRAP analysis of FLAG-EGFP (FE)-tagged PALB2 WT, 7Q, and 7R dynamics in U2OS Flp-In T-Rex cells in which endogenous PALB2 was depleted via RNA interference. For each cell line, representative images of live cells before bleaching (pre-bleaching) and during the recovery period (post-bleaching) are shown together with half-time recovery plots for at least 20 cells. Dashed circles indicate bleached areas. Statistical analyses were performed using GraphPad Prism 7.02 and *p*-values are for the unpaired Student's *t*-test (**** $p < 0.0001$).

Figure 5. **The ChAM 7K-patch is required for PALB2 function in genome stability maintenance.** ***A***. Western blot analysis of FLAG-PALB2 and BRCA2 levels in U2OS Flp-In T-Rex cells stably expressing FLAG (EV) and FLAG-PALB2 WT, 7Q, or 7R. Where indicated, cells were treated with 2 μg/mL doxycycline (Dox) to induce endogenous PALB2 depletion. Lamin was used as a loading control. ***B-C.*** Representative images showing RAD51 foci (B), and plot presenting the number of RAD51 foci per cell (C) in U2OS Flp-In T-Rex cells ($n \geq 62$) stably expressing FLAG (EV) and FLAG-PALB2 WT, 7Q, or 7R, following Dox-induced endogenous PALB2 depletion and treatment with 4 Gy of IR. DAPI was used for nuclear staining and γ-H2AX as a marker for DNA damage (B). Statistical analyses were performed using GraphPad Prism 7.02 and *p*-values are for the unpaired

Student's *t*-test (**** $p < 0.0001$). ***D.*** Cell survival following Olaparib treatment of U2OS Flp-In T-Rex cells stably expressing FLAG (EV) and FLAG-PALB2 WT, 7Q, or 7R. Where indicated Dox was used to induce endogenous PALB2 depletion. The percentage of live cells was assessed by WST-1 assay after five days of Olaparib treatment.

Figure 6. **Model for PALB2 acetylation function in the maintenance of genome stability**. ***Left***: MRG15 and KAT2A/B-mediated ChAM acetylation jointly promote PALB2 enrichment at undamaged transcriptionally active chromatin. DNA damage triggers ChAM deacetylation and releases PALB2 from chromatin. This allows PALB2 to interact with BRCA1, which in turn recruits the entire HR complex to sites of DNA damage. ChAM binding to naked DNA through the 7K-patch may promote RAD51 loading and HR repair. ***Right***: The 7K-patch null mutant with K to Q substitutions is more freely diffusible, and although it can be recruited to sites of DNA damage, it fails to engage with damaged DNA, leading to defective HR.

Supplementary Figure 1. PALB2 dynamics increases upon DNA damage or deacetylation. ***A***. γ-H2AX levels in untreated or damaged cells (4 Gy of ionising radiation (IR), 1 mM of mitomycin C (MMC), or 2.5 μM of Olaparib) as measured by anti-γ-H2AX immunofluorescence staining. ***B***. Relative fluorescence intensity of FE-PALB2 in either undamaged or DNA damaging conditions (4 Gy of IR or 1 mM of MMC) measured after photobleaching of cells shown in Fig. 1 A, B. ***C.*** Relative fluorescence intensity of FE-PALB2 in either undamaged (DMSO vehicle) or DNA damaging conditions (2.5 μM Olaparib) measured after photobleaching of cells shown in Fig. 1C, D. ***D***. KAT2A protein levels measured by western blot analysis of U2OS Flp-In T-Rex FE-PALB2 cells treated with small RNA interference targeting KAT2A and KAT2B (siKAT2A/siKAT2B) or

scramble small interfering RNA (siCntl) (negative control) for either 48 or 72 h. Tubulin was used as a loading control. ***E***. Relative fluorescence intensity of FE-PALB2 in WT, siSCR, and siKAT2A/B conditions, related to FRAP analysis shown in Fig. 1E, F. ***F***. Level of pan-acetylated histones in U2OS Flp-In T-Rex FE-PALB2 cells treated with DMSO or deacetylases inhibitors (KDACi). Ponceau staining of proteins after transfer onto nitrocellulose membrane was used as a loading control. ***G***. Relative fluorescence intensity of FE-PALB2 in mock and KDACi conditions, related to FRAP analysis shown in Fig. 1G, H.

Supplementary Figure 2. PALB2 is acetylated by KAT2 within ChAM, which is deacetylated upon DNA damage. ***A-B.*** *In vitro* acetylation of PALB2 by KAT2B (panel A) or KAT2A and a catalytically inactive mutant, KAT2A-ED (panel B). Purified PALB2 full-length and fragments 1-4 (Fig. 2A) were incubated with either purified FLAG-KAT2B, FLAG-KAT2A, or FLAG-KAT2A-ED in the presence of acetyl-CoA and then separated by SDS-PAGE. Protein content was visualised by Ponceau staining, and acetylated proteins were detected by anti-acetyl lysine (pan-AcK) western blot. Acetylation of PALB2 fragment 2 by active KAT2B or KAT2A is highlighted by red dotted boxes.

Supplementary Figure 3. FRAP analysis of FE-PALB2 harbouring an internal deletion of the ChAM. ***A-C***. FRAP analysis of FE-PALB2 wild-type (WT) or harbouring an internal deletion of the ChAM (ΔChAM). Images of FE-PALB2 in live cells before bleaching (pre-bleaching) and during the recovery time after bleaching are shown (panel A), together with plots of half-time recovery times (s) after photobleaching (panel B) and relative fluorescence intensity (panel C).

Supplementary Figure 4. The ChAM 7K-patch controls PALB2 chromatin association. ***A.*** Chemical structure of side-chains of lysine (K), acetylated lysine (K-ac), arginine (R), and glutamine (Q) residues, showing differences in size and charge for each residue. ***B.*** Cellular distribution of FLAG-PALB2 WT, 7Q, and 7R between cytoplasmic (Cyt), nuclear soluble (Nu), and chromatin-enriched (Chr) fractions from U2OS Flp-In T-Rex cells stably expressing either FLAG (EV) or FLAG-PALB2 WT, 7Q, or 7R upon PALB2 depletion induced by doxycycline treatment (2 μg/mL). Chromatin association was analysed by anti-FLAG western blot, and Histone H3 was used as a control for cellular fractionation. ***C.*** Level of FLAG-PALB2 WT, 7Q, and 7R in the chromatin fraction of U2OS Flp-In T-Rex cells stably expressing either FLAG (EV) or FLAG-PALB2 WT, 7Q, or 7R. The quantification was performed by densitometry analyses using Image J. PALB2 levels in the chromatin fraction were normalized to PALB2 levels in whole-cell extracts and expressed as a percentage of the WT. Statistical analyses were performed using GraphPad Prism 7.02, and *p*-values are for the unpaired Student's *t*-test (**** $p < 0.0001$, ns = non-specific). ***D.*** Analysis of FE-PALB2 WT, 7R, and 7Q temporal recruitment to DNA damage sites induced by laser micro-irradiation. Dashed boxes indicate damaged areas. ***E.*** Quantitation of the amount of FE-PALB2 WT, 7R, and 7Q recruited to laser damage sites. The relative fluorescence intensity at laser damage sites was calculated by dividing the fluorescence intensity of the damaged area over the time course experiment by the fluorescence intensity of the non-damaged region of the nucleus and normalisation using the pre-damaged fluorescence value as a reference.

Supplementary Figure 5. PALB2 ChAM 7K-patch is required to maintain genome stability. ***A.*** Number of RAD51 foci per cell in WT U2OS Flp-In T-Rex cells (-Dox) or cells depleted for PALB2 (+Dox), in either untreated or DNA damaging conditions (1 mM of

MMC or 4 Gy of IR). ***B.*** FLAG-PALB2 was pulled-down from U2OS Flp-In T-Rex cells stably expressing either FLAG-PALB2 WT, 7Q, or 7R, following endogenous PALB2 depletion induced by doxycycline treatment (2 µg/mL). Cells expressing only the FLAG-tag (EV) were used a negative control. BRCA2 and RAD51 interaction with PALB2 was assessed by anti-BRCA2 and anti-RAD51 western blot, respectively.

References

1. Xia, B. et al. Control of BRCA2 cellular and clinical functions by a nuclear partner, PALB2. *Mol Cell* **22**, 719-29 (2006).
2. Reid, S. et al. Biallelic mutations in PALB2 cause Fanconi anemia subtype FA-N and predispose to childhood cancer. *Nat Genet* **39**, 162-4 (2007).
3. Xia, B. et al. Fanconi anemia is associated with a defect in the BRCA2 partner PALB2. *Nat Genet* **39**, 159-61 (2007).
4. Rahman, N. et al. PALB2, which encodes a BRCA2-interacting protein, is a breast cancer susceptibility gene. *Nat Genet* **39**, 165-7 (2007).
5. Jones, S. et al. Exomic sequencing identifies PALB2 as a pancreatic cancer susceptibility gene. *Science* **324**, 217 (2009).
6. O'Donovan, P.J. & Livingston, D.M. BRCA1 and BRCA2: breast/ovarian cancer susceptibility gene products and participants in DNA double-strand break repair. *Carcinogenesis* **31**, 961-7 (2010).
7. Sy, S.M., Huen, M.S. & Chen, J. PALB2 is an integral component of the BRCA complex required for homologous recombination repair. *Proc Natl Acad Sci U S A* **106**, 7155-60 (2009).
8. Bleuyard, J.Y. et al. MRG15-mediated tethering of PALB2 to unperturbed chromatin protects active genes from genotoxic stress. *Proc Natl Acad Sci U S A* **114**, 7671-7676 (2017).
9. Hayakawa, T. et al. MRG15 binds directly to PALB2 and stimulates homology-directed repair of chromosomal breaks. *J Cell Sci* **123**, 1124-30 (2010).
10. Sy, S.M., Huen, M.S. & Chen, J. MRG15 is a novel PALB2-interacting factor involved in homologous recombination. *J Biol Chem* **284**, 21127-31 (2009).
11. Bleuyard, J.Y., Buisson, R., Masson, J.Y. & Esashi, F. ChAM, a novel motif that mediates PALB2 intrinsic chromatin binding and facilitates DNA repair. *EMBO Rep* **13**, 135-41 (2012).
12. Bleuyard, J.Y., Butler, R.M. & Esashi, F. Perturbation of PALB2 function by the T413S mutation found in small cell lung cancer. *Wellcome Open Res* **2**, 110 (2017).
13. Dantuma, N.P. & van Attikum, H. Spatiotemporal regulation of posttranslational modifications in the DNA damage response. *EMBO J* **35**, 6-23 (2016).
14. Guo, Y., Feng, W., Sy, S.M. & Huen, M.S. ATM-dependent Phosphorylation of the Fanconi Anemia Protein PALB2 Promotes the DNA Damage Response. *J Biol Chem* **290**, 27545-56 (2015).
15. Ahlskog, J.K., Larsen, B.D., Achanta, K. & Sorensen, C.S. ATM/ATR-mediated phosphorylation of PALB2 promotes RAD51 function. *EMBO Rep* **17**, 671-81 (2016).

16. Buisson, R. et al. Coupling of Homologous Recombination and the Checkpoint by ATR. *Mol Cell* **65**, 336-346 (2017).
17. Orthwein, A. et al. A mechanism for the suppression of homologous recombination in G1 cells. *Nature* **528**, 422-6 (2015).
18. Fournier, M. et al. KAT2A/KAT2B-targeted acetylome reveals a role for PLK4 acetylation in preventing centrosome amplification. *Nat Commun* **7**, 13227 (2016).
19. Nagy, Z. et al. The metazoan ATAC and SAGA coactivator HAT complexes regulate different sets of inducible target genes. *Cell Mol Life Sci* **67**, 611-28 (2010).
20. Tanner, K.G., Langer, M.R. & Denu, J.M. Kinetic mechanism of human histone acetyltransferase P/CAF. *Biochemistry* **39**, 11961-9 (2000).
21. Wellen, K.E. et al. ATP-citrate lyase links cellular metabolism to histone acetylation. *Science* **324**, 1076-80 (2009).
22. Nowell, P.C. The clonal evolution of tumor cell populations. *Science* **194**, 23-8 (1976).
23. Yata, K. et al. BRCA2 coordinates the activities of cell-cycle kinases to promote genome stability. *Cell Rep* **7**, 1547-1559 (2014).
24. Schindelin, J. et al. Fiji: an open-source platform for biological-image analysis. *Nat Methods* **9**, 676-82 (2012).
25. Schneider, C.A., Rasband, W.S. & Eliceiri, K.W. NIH Image to ImageJ: 25 years of image analysis. *Nat Methods* **9**, 671-5 (2012).
26. Yu, D.S. et al. Dynamic control of Rad51 recombinase by self-association and interaction with BRCA2. *Mol Cell* **12**, 1029-41 (2003).
27. Srivastava, V. et al. BLM helicase stimulates the ATPase and chromatin-remodeling activities of RAD54. *J Cell Sci* **122**, 3093-103 (2009).
28. Jeyasekharan, A.D. et al. DNA damage regulates the mobility of Brca2 within the nucleoplasm of living cells. *Proc Natl Acad Sci U S A* **107**, 21937-42 (2010).
29. Kulak, N.A., Pichler, G., Paron, I., Nagaraj, N. & Mann, M. Minimal, encapsulated proteomic-sample processing applied to copy-number estimation in eukaryotic cells. *Nat Methods* **11**, 319-24 (2014).
30. Hein, M.Y. et al. A human interactome in three quantitative dimensions organized by stoichiometries and abundances. *Cell* **163**, 712-23 (2015).
31. Lee, J.V. et al. Akt-dependent metabolic reprogramming regulates tumor cell histone acetylation. *Cell Metab* **20**, 306-319 (2014).
32. Perez-Riverol, Y. et al. The PRIDE database and related tools and resources in 2019: improving support for quantification data. *Nucleic Acids Res* **47**, D442-D450 (2019).

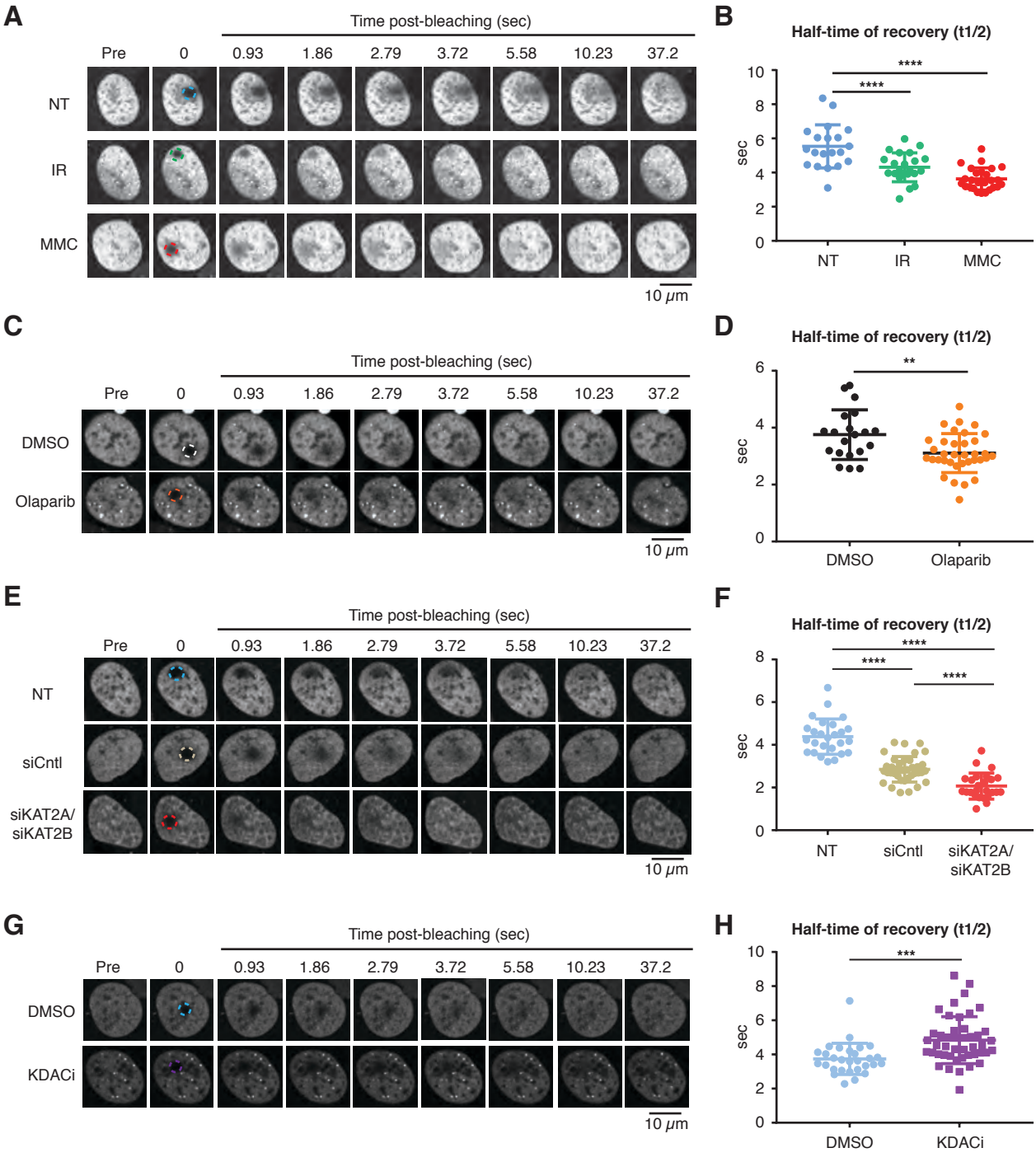
A
Time post-bleaching (sec)
Pre
0
0.93
1.86
2.79
3.72
5.58
10.23
37.2
NT
IR
MMC
10 μm
B
Half-time of recovery (t1/2)
****
****
sec
NT
IR
MMC
C
Time post-bleaching (sec)
DMSO
Olaparib
10 μm
D
Half-time of recovery (t1/2)
**
DMSO
Olaparib
E
Time post-bleaching (sec)
NT
siCntl
siKAT2A/
siKAT2B
10 μm
F
Half-time of recovery (t1/2)
****
****
****
NT
siCntl
siKAT2A/
siKAT2B
G
Time post-bleaching (sec)
DMSO
KDACi
10 μm
H
Half-time of recovery (t1/2)
***
DMSO
KDACi

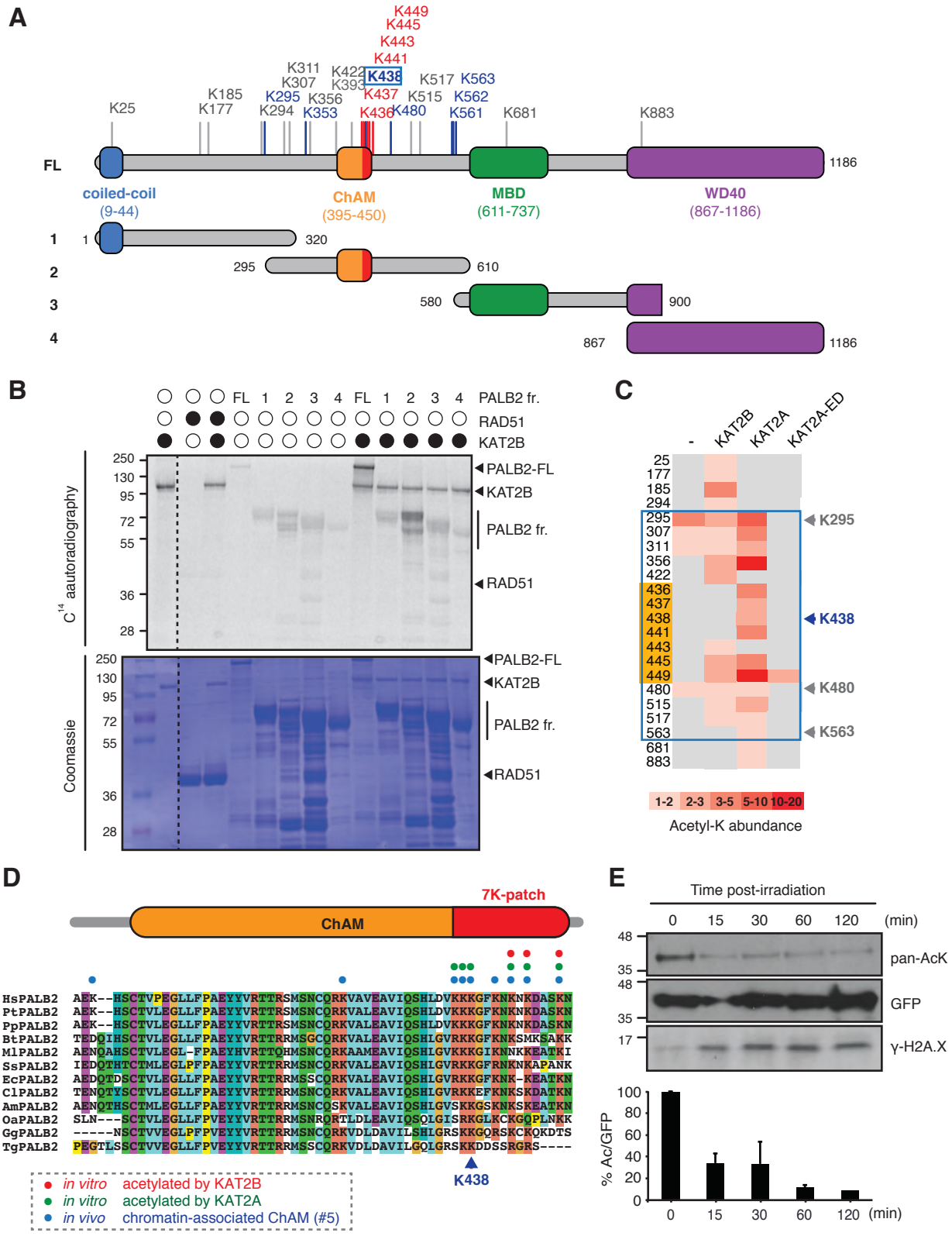
A
K449
K445
K443
K441
K438
K437
K436
K311
K307
K422
K393
K517
K563
K185
K177
K295
K294
K356
K353
K515
K562
K561
K480
K681
K883
K25
FL
1186
coiled-coil
(9-44)
ChAM
(395-450)
MBD
(611-737)
WD40
(867-1186)
1
1
320
2
295
610
3
580
900
4
867
1186
B
FL 1 2 3 4 FL 1 2 3 4
PALB2 fr.
RAD51
KAT2B
C14 autoradiography
250
130
95
72
55
36
28
PALB2-FL
KAT2B
PALB2 fr.
RAD51
Coomassie
250
130
95
72
55
36
28
PALB2-FL
KAT2B
PALB2 fr.
RAD51
C
-
KAT2B
KAT2A
KAT2A-ED
25
177
185
294
295
307
311
356
422
436
437
438
441
443
445
449
480
515
517
563
681
883
K295
K438
K480
K563
1-2
2-3
3-5
5-10
10-20
Acetyl-K abundance
D
7K-patch
ChAM
HsPALB2 AEK--HSCTVPEGLLFPAEYYVRTTRSMSNCQRKVAVEAVIQSHLDVKKKGFKNKNKDASKN
PtPALB2 AEK--HSCTVLEGLLFPAEYYVRTTRSMSNCQRKVALEAVIQSHLDVKKKGFKNKNKDASKN
PpPALB2 AEK--HSCTVLEGLLFPAEYYVRTTRSMSNCQRKVALEAVIQSHLDVKKKGFKNKNKDASKN
BtPALB2 TEDQIHSCTVLEGLLFPAEYYVRTTRRMSGCQRKVALEAVIQSHLGVRKKGFKNKSMKSAKK
MlPALB2 AENQAHSCTVLEGL-FPAEYHVRTTQHMSNCQRKAAMEAVIQSHLGVKKKGIKNNKKEATKI
SsPALB2 IEDQTHTCTMLEGLPFPAEYYVRTTRRMSNCQRKVALEAVIQSHLGVRKKGFRNKNKAPANK
EcPALB2 AEDQTDSCTVLEGLLFPAEYYVRTTRRMSSCQRKVALEAVIQSHLGVRKKGFKNK-KEATKN
ClPALB2 TENQTYSCTVLEGLLFPAEYYVRTTRRMSNCQRKVALEAVIQSHLGVRKKEFKNKSKDATKN
AmPALB2 AENQTHSCTMLEGLLFPAEYYVRTTRRMSNCQSKVALEAVIQSHLGVSKKGSKNKSKEATKN
OaPALB2 SLN---SCTVLEGLLFPVEYYVRTTRRMSNRQRTLDLEAVIQSQLGISRKGLKCKGQPLNKK
GgPALB2 -----NSCTVVEGLPFPVEYYVRTTRRMSNCQRKVDLDAVILSHLGRSKKGQRSKCKQKDTS
TgPALB2 PEGTLSSCTVVEGLLFPVEYYVRTTRRMSSCQRKVDLDAVILGQLGRSKKDDSSRGRS----
K438
in vitro acetylated by KAT2B
in vitro acetylated by KAT2A
in vivo chromatin-associated ChAM (#5)
E
Time post-irradiation
0 15 30 60 120 (min)
48
35
48
35
17
pan-AcK
GFP
γ-H2A.X
100
80
60
40
20
0
% Ac/GFP
0 15 30 60 120 (min)

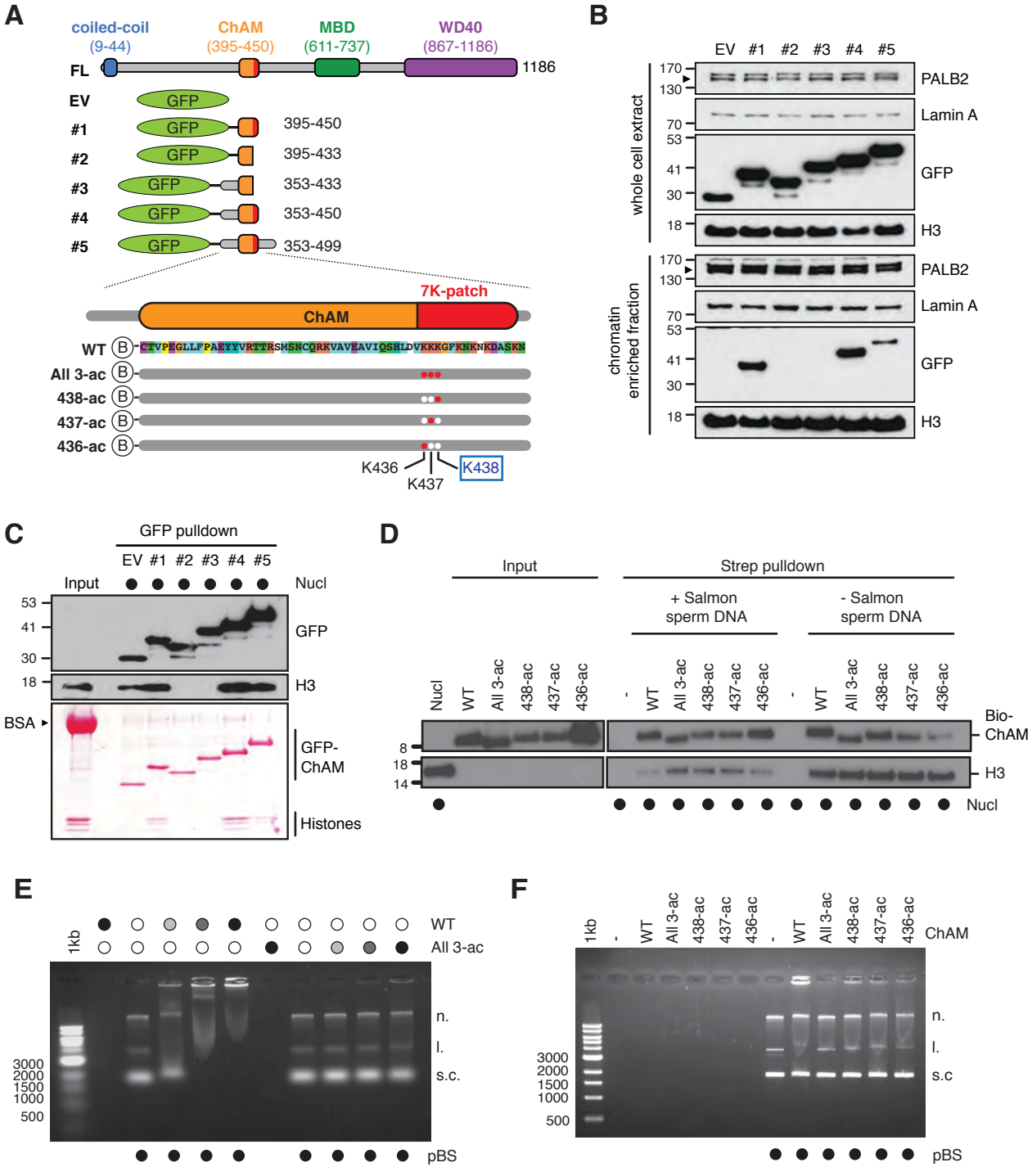
A
coiled-coil
(9-44)
ChAM
(395-450)
MBD
(611-737)
WD40
(867-1186)
FL
1186
EV
GFP
#1
395-450
#2
395-433
#3
353-433
#4
353-450
#5
353-499
7K-patch
ChAM
WT
All 3-ac
438-ac
437-ac
436-ac
K436
K437
K438
B
EV #1 #2 #3 #4 #5
whole cell extract
chromatin enriched fraction
PALB2
Lamin A
GFP
H3
170
130
70
53
41
30
18
C
GFP pulldown
EV #1 #2 #3 #4 #5
Input
Nucl
GFP
H3
BSA
GFP-ChAM
Histones
D
Input
Strep pulldown
+ Salmon sperm DNA
- Salmon sperm DNA
Nucl
WT
All 3-ac
438-ac
437-ac
436-ac
Bio-ChAM
H3
8
18
14
E
1kb
WT
All 3-ac
n.
l.
s.c.
3000
2000
1500
1000
500
pBS
F
ChAM
n.
l.
s.c
pBS

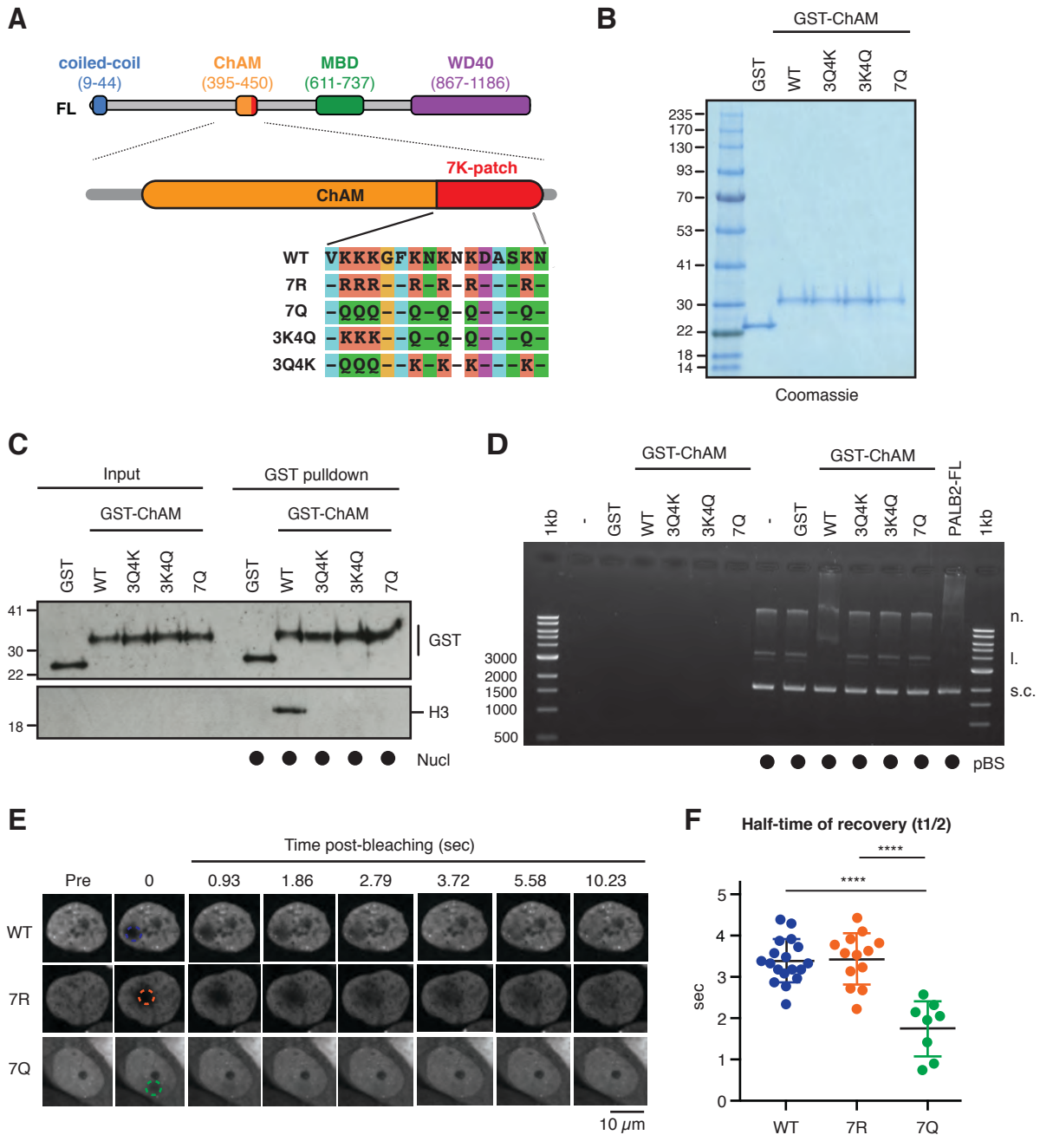
A
coiled-coil
(9-44)
ChAM
(395-450)
MBD
(611-737)
WD40
(867-1186)
FL
7K-patch
ChAM
WT VKKKGFKNKNKDASKN
7R -RRR--R-R-R---R-
7Q -QQQ--Q-Q-Q---Q-
3K4Q -KKK--Q-Q-Q---Q-
3Q4K -QQQ--K-K-K---K-
B
GST-ChAM
GST
WT
3Q4K
3K4Q
7Q
235
170
130
93
70
53
41
30
22
18
14
Coomassie
C
Input
GST pulldown
GST-ChAM
GST-ChAM
GST
WT
3Q4K
3K4Q
7Q
41
30
22
18
GST
H3
Nucl
D
GST-ChAM
GST-ChAM
1kb
-
GST
WT
3Q4K
3K4Q
7Q
PALB2-FL
3000
2000
1500
1000
500
n.
l.
s.c.
pBS
E
Time post-bleaching (sec)
Pre
0
0.93
1.86
2.79
3.72
5.58
10.23
WT
7R
7Q
10 μm
F
Half-time of recovery (t1/2)
****
****
sec
5
4
3
2
1
0
WT
7R
7Q

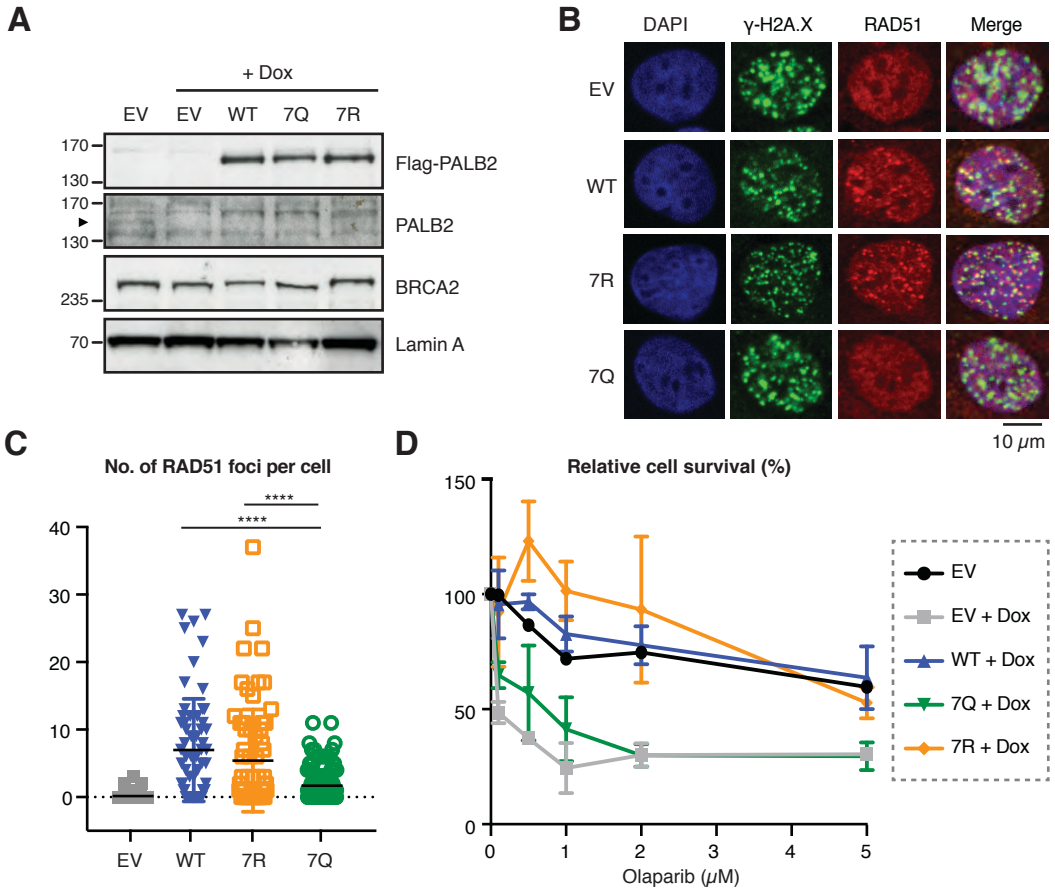
A
+ Dox
EV EV WT 7Q 7R
170
130
170
130
235
70
Flag-PALB2
PALB2
BRCA2
Lamin A
B
DAPI
γ-H2A.X
RAD51
Merge
EV
WT
7R
7Q
10 μm
C
No. of RAD51 foci per cell
****
****
40
30
20
10
0
EV WT 7R 7Q
D
Relative cell survival (%)
150
100
50
0
0 1 2 3 4 5
Olaparib (μM)
EV
EV + Dox
WT + Dox
7Q + Dox
7R + Dox

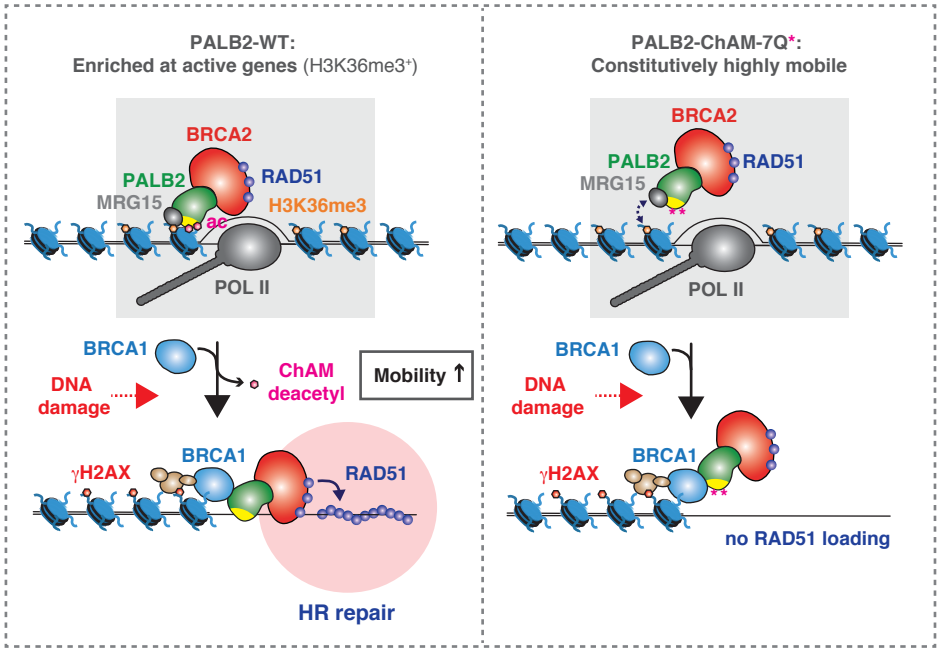
PALB2-WT:
Enriched at active genes (H3K36me3+)
BRCA2
PALB2
RAD51
MRG15
H3K36me3
ac
POL II
BRCA1
DNA damage
ChAM deacetyl
Mobility ↑
γH2AX
BRCA1
RAD51
HR repair
PALB2-ChAM-7Q*:
Constitutively highly mobile
BRCA2
PALB2
RAD51
MRG15
POL II
BRCA1
DNA damage
γH2AX
BRCA1
no RAD51 loading

MF *et al*_Supplementary Figure 1

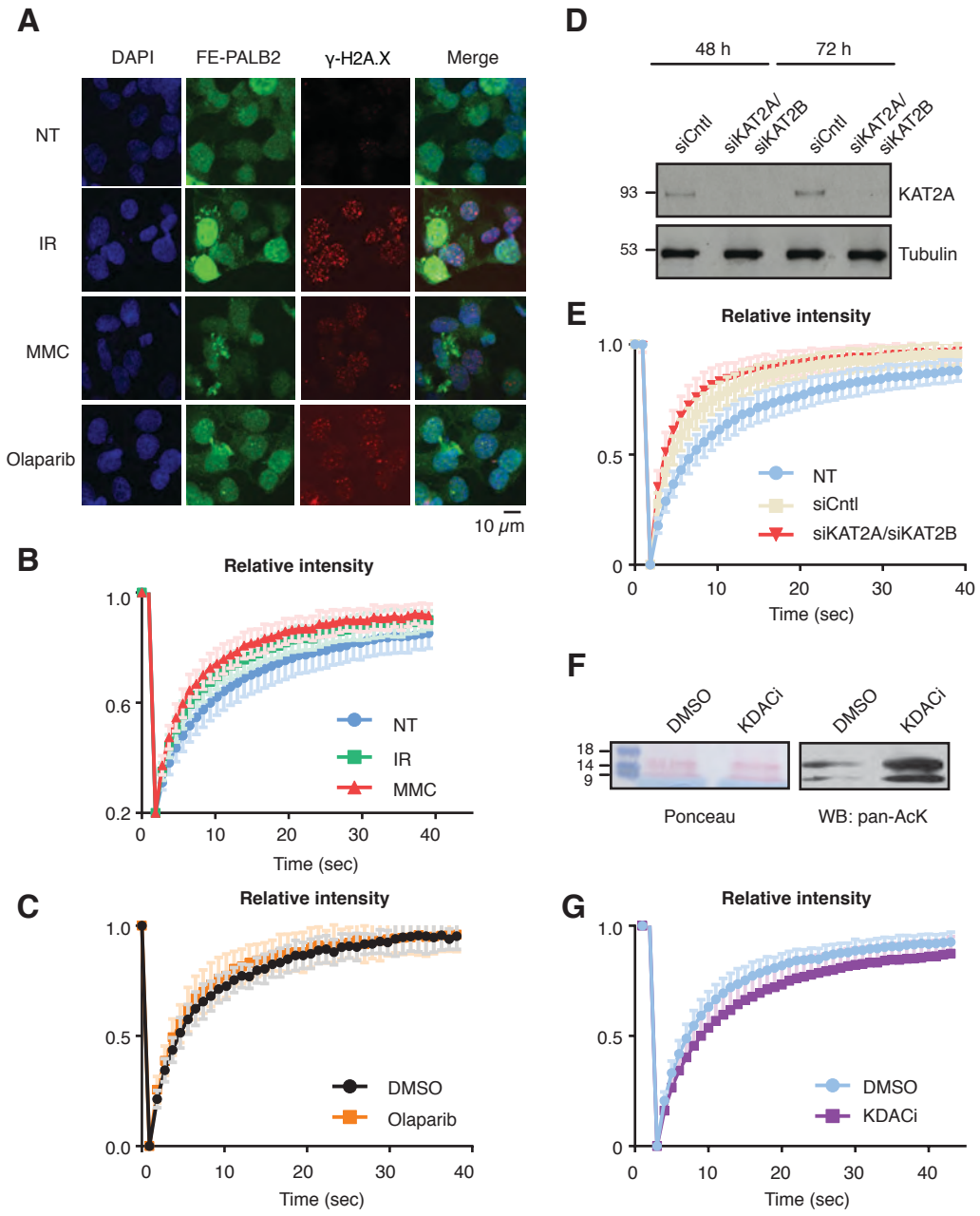

MF *et al*_Supplementary Figure 2

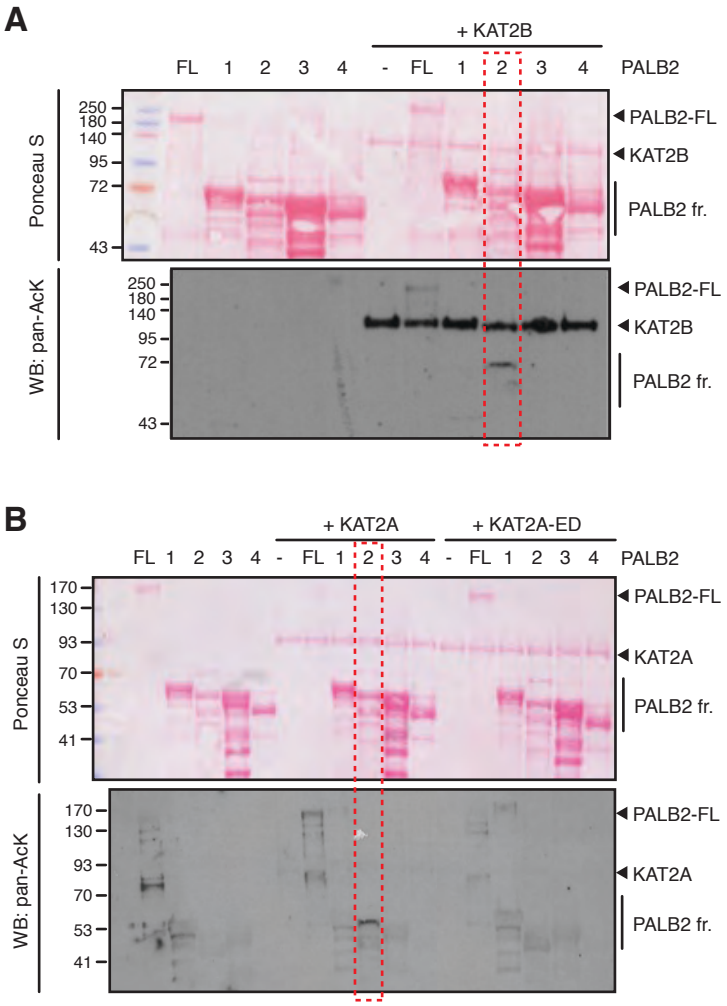

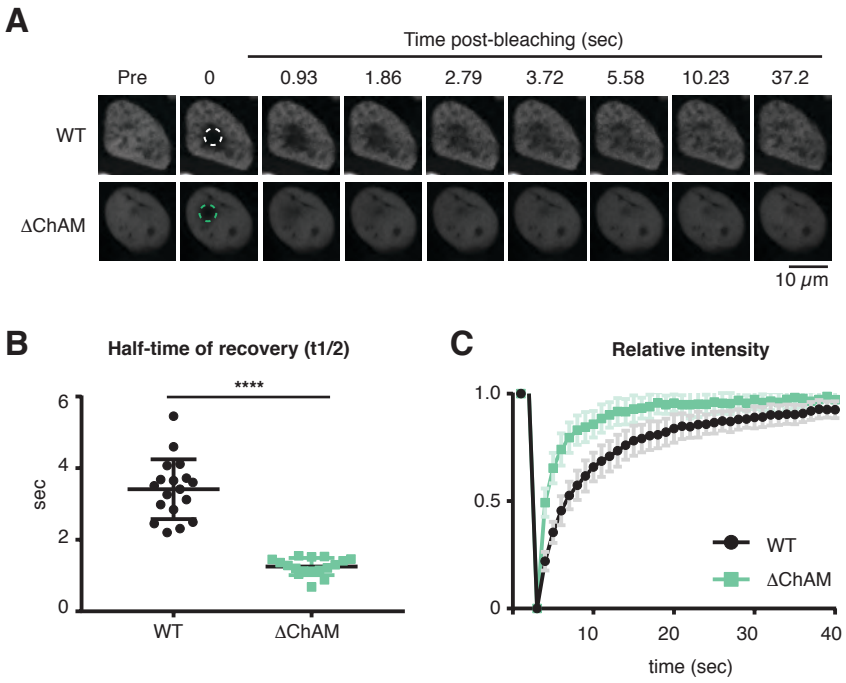
A
Time post-bleaching (sec)
Pre
0
0.93
1.86
2.79
3.72
5.58
10.23
37.2
WT
ΔChAM
10 μm
B
Half-time of recovery (t1/2)
****
sec
6
4
2
0
WT
ΔChAM
C
Relative intensity
1.0
0.5
0
10
20
30
40
time (sec)
WT
ΔChAM

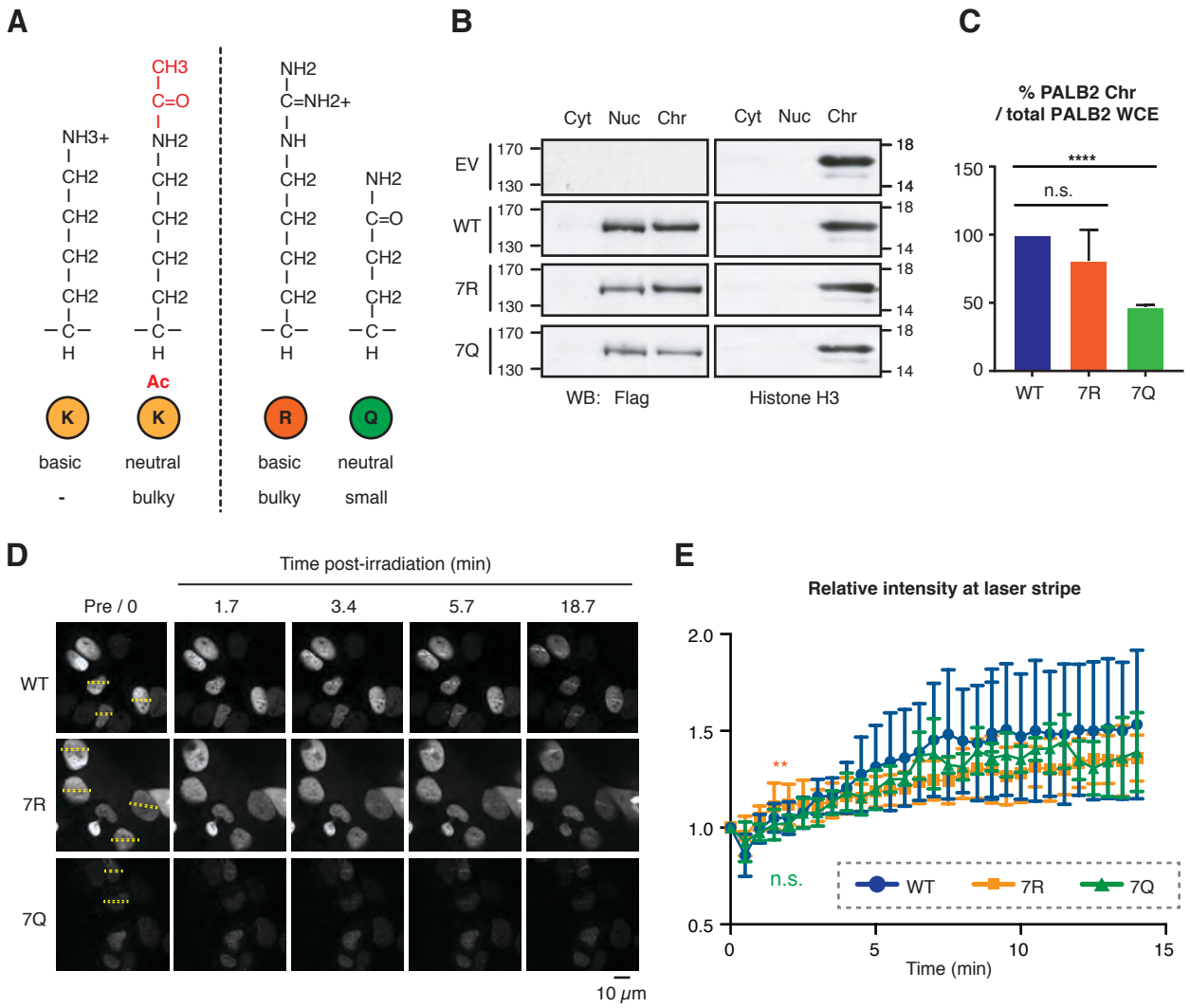
A
NH3+
CH2
CH2
CH2
CH2
C
H
CH3
C=O
NH2
CH2
CH2
CH2
CH2
C
H
Ac
K
K
basic
neutral
-
bulky
NH2
C=NH2+
NH
CH2
CH2
CH2
CH2
C
H
NH2
C=O
CH2
CH2
C
H
R
Q
basic
neutral
bulky
small
B
Cyt Nuc Chr
Cyt Nuc Chr
EV
WT
7R
7Q
170
130
18
14
WB: Flag
Histone H3
C
% PALB2 Chr
/ total PALB2 WCE
****
n.s.
150
100
50
0
WT
7R
7Q
D
Time post-irradiation (min)
Pre / 0
1.7
3.4
5.7
18.7
WT
7R
7Q
10 μm
E
Relative intensity at laser stripe
2.0
1.5
1.0
0.5
**
n.s.
WT
7R
7Q
0
5
10
15
Time (min)

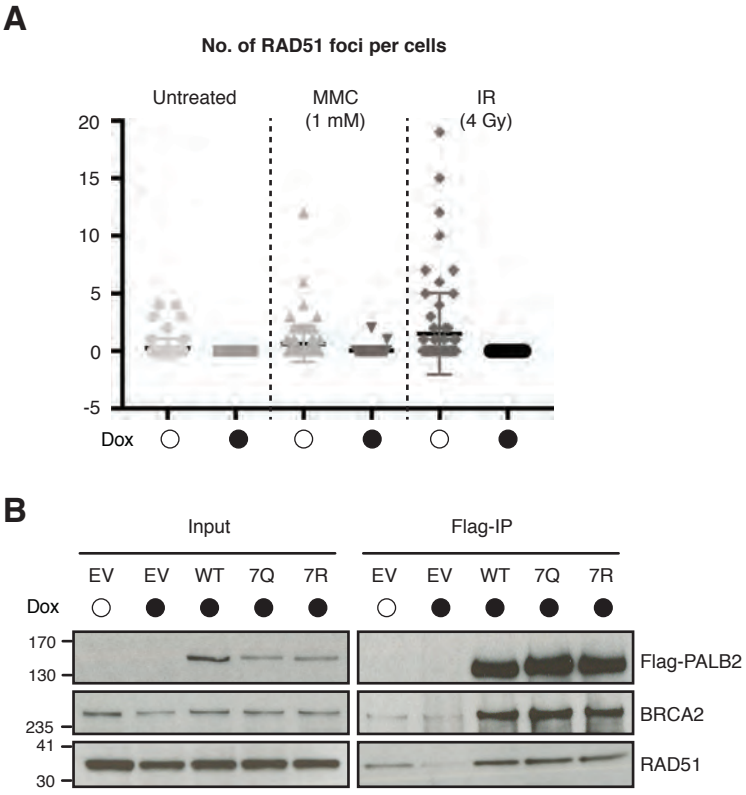
A
No. of RAD51 foci per cells
Untreated
MMC
(1 mM)
IR
(4 Gy)
20
15
10
5
0
-5
Dox
B
Input
Flag-IP
EV
EV
WT
7Q
7R
EV
EV
WT
7Q
7R
Dox
170
130
235
41
30
Flag-PALB2
BRCA2
RAD51